

An Algebraic Approach for the Stability Analysis of BLDC Motor Controllers

Julio C. G. Pimentel, *Senior Member, IEEE*, Emad Gad, *Senior Member, IEEE*,

Abstract—This paper presents an algebraic technique to compute the maximum time-delay that can be accepted in the control loop of a Brushless DC Motor (BLDCM) speed controller before the closed loop response becomes unstable. Using a recently proposed time-delay stability analysis methodology, we derive accurate stability conditions for the BLDCM speed controller. The results of applying the new method show that tuning the PI controller for very fast response in the order of magnitude of the BLDCM mechanical time constant cause the time-delay to significantly affect the system stability.

Index Terms—Stability, Electric Differential, Electric Vehicle, High Speed Spindle, Motor Control, BLDC, High Speed Motor.

I. INTRODUCTION

IN the last decade, the brushless direct current motors (BLDCM) became widely used in a variety of applications due to its robust mechanical topology and simplicity of control, higher speed of operation, higher torque for the same power density and lower manufacturing cost compared to existing frequency controlled AC drives and vector controlled permanent magnet synchronous motors (PMSM). They have also become widely used in low power and high speed applications creating a need for efficient and low cost controllers [1] [2]. BLDC motors are also used in energy related applications such as hybrid vehicles integrated starter-generator, fuel pumps and electric differential [3] [4] [5], consumer appliances, computer numerical control, drilling tools, small hydro and wind energy generation, and flywheel energy-storage systems [6] [7].

Nonetheless, the industrial potentials of the BLDCM pose new challenges for the close-loop control design that were not seen with the controllers of classical motors. One such challenge arises from the small mechanical time constant (τ_{mech}), which typically approaches the order of few milliseconds. With such a small time constant, the total time delay in the controller (τ_{total}) induced by the various modules in the closed-loop becomes a dominant player in determining the stability of the controller.

The question of whether a closed-loop controller with a particular delay value is stable or not is easily answered through the classical graphical methods on Bode or Nyquist plots [8] [9]. However, in the context of the BLDCM, the more fitting question to ask is: *how much total delay can be tolerated in the closed-loop before the system exhibits unstable behaviour?* The lack of a satisfactory, accurate and simple method to answer that question typically forces the motion control designer to use conservative tuning scheme, a

practice that often times comes at the expense of slowing down the response of the set-point tracking or the load-disturbance rejection.

The purpose of this paper is to present a simple algebraic approach to answer the above question. More precisely, the proposed method enables computing the maximum delay τ_{max} that can be allowed in the control loop while maintaining the desired margins of stability in the system.

The immediate benefit gained from the new method of the proposed method is that it provides, so to speak, a new lens through which commonly used PI-controller tuning methodologies can be viewed and assessed. Indeed, as will be shown in this paper, the proposed approach offers new insights in the famous tuning methodologies that remained hitherto unknown. The long-term benefits of the proposed method is that it opens the door to new automatic tuning strategies that take into account the actual values of τ_{total} and τ_{max} in tuning the controller parameters.

The proposed method is based on a recent approach, initially proposed in [10], and later extended in [11], to derive the stability condition of a linear time invariant retarded time-delay system (LTI-RTDS). The proposed technique constructs an analytical model for the controller of the BLDCM set-point tracking and load-disturbance rejection transfer functions that takes into account the various sources of delay in the control loop. It then adapts the method of [11] to estimate the maximum delay, τ_{max} that can be tolerated in the loop before the system becomes unstable. Subsequently, τ_{max} arising from commonly-used PI controller tuning methodologies is computed, and used to shed the light on the performance of the tuning methodology. Future works will use the proposed method to derive a systematic procedure to tune the controller parameters to achieve a more optimized performance.

The rest of the paper is organized as follows. Section III presents a quick summary of the time-delay analysis method used. Section IV briefly develops the BLDCM state space model and identifies various sources of delay affecting the controller stability and presents the development of the BLDCM models with time-delays. Section V derives the stability conditions and analyzes the effect of the delay on the stability of the closed-loop control system. In section VI we analyze the effect on the stability condition of varying the controller parameters. Finally, section VII presents the test bench built to validate the results including simulated and measured results.

J. C. G. Pimentel (e-mail: pimentel@ieee.org) is with

E. Gad is with SITE, University of Ottawa, Ottawa, ON, CA, e-mail: egad@uottawa.ca.

II. BACKGROUND, MOTIVATION AND PROBLEM FORMULATION

This section sets the stage for the problem scope addressed by the work presented in this paper. It also lays out the motivation the relevant mathematical problems formulation.

A. Problem Scope

Fig. 1 depicts a representation of the scope of the problem addressed by the approach presented in this work. The plane in the block diagram of Fig. 1 represents the BLDC moto and the PI block represents the Proportional-Integrator controller module. The transfer function of the plant may include certain elements that cause a pure delay which is taken into account by expressing the transfer function as a function of two variables s and $e^{-s\tau_2}$. Likewise the PI controller may also include a delay $e^{-s\tau_1}$ in addition to the classical proportional and integrator constants k_p and k_i , respectively. The feedback path is also a delay-dependent transfer function $G_c(s, e^{-s\tau_3})$

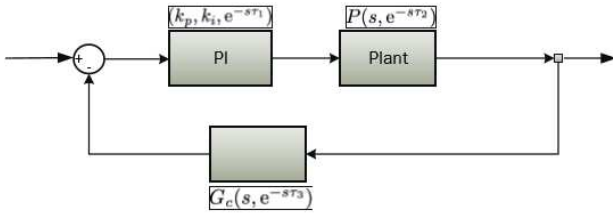


Fig. 1. PI-based control with several delay sources.

The delays in the above components are assumed to be characterized by uncertainty or may alternatively be regarded as shifting with time in an unspecified way. Those delays arise not from design decisions, but only as second-order effect from the system hardware or wiring.

It is also assumed that absent those sources of delays, $\tau_1 = \tau_2 = \tau_3 = 0$, the close-loop control system is stable. On the other hand, the presence of the delays, i.e. $\tau_i > 0$ may, or may not, render the system unstable. However, it is not the main concern in this paper to determine whether the system is stable for particular values of the delays. Rather, the main concerns in this work can be summed up by the following questions:

- 1) Is there a limit, efficiently computable, for those delays beyond which, the system becomes unstable.
- 2) If that limit is found to exist, then how is this limit compared with the actual delays in the circuit.
- 3) Denoting the difference between the limit and actual delays in the system by the so-called *delay margin*, what is the impact of k_p and k_i on the delay margin.

B. Motivations

In many systems depicted by the block diagram of Fig. 1, the actual delays are negligible in comparison with the time constants of the mechanical dynamics of the system. Indeed, these situations do not warrant the investigations by the methods proposed in this work. However, in the case of the BLDC motors, the mechanical time constants is sufficiently small that the delays in the closed-loop control system is a

sizeable portion from it. Under those conditions, the delay margin becomes an important factor to take into account in designing or tuning the PI parameters k_p and k_i . For example, a desirable PI design would be one that maximizes the delay margin to guard against potential delay-caused instability but not at the expense of slowing down the system extensively.

The foremost goal of this work is to develop a simple algebraic method that maps the various design parameters, including the parameters k_p and k_i , to the delay margin of the system. The proposed method will used to take a new look at the existing PI design tuning methodologies and show through experimental results their impact on the system performance.

C. Mathematical Problem Formulation

The mathematical model that represents the close-loop BLDC motor problem is cast as a system of linear time-invariant retarded time-delay system (LTI-RTDS) that takes the following form

$$\frac{d\mathbf{x}(t)}{dt} = \mathbf{A}_0\mathbf{x}(t) + \mathbf{A}_1\mathbf{x}(t - \tau) + \mathbf{B}\mathbf{u}(t) \quad (1)$$

The derivation of the above formulation for the underlying system will detailed in Section IV. The parameters in (1) are defined as follows. $\mathbf{x}(t) \in \mathbb{R}^n$ is the state-space vector, \mathbf{A}_0 and $\mathbf{A}_1 \in \mathbb{R}^{n \times n}$ are real coefficient matrices with ranks n, N , respectively, ($N \leq n$), $\tau \in \mathbb{R}^+$ is a parameter that represents the delay in the system, $\mathbf{B} \in \mathbb{R}^{n \times p}$ is the input matrix and $\mathbf{u}(t) \in \mathbb{R}^p$ is called the input (or control) vector.

The system is assumed to be stable without delay, i.e., if $\tau = 0$. One must also note here that the delay parameter τ in (1) is the actual delay, that is, it is a delay introduced (inadvertently) by the various modules in the closed-loop control system. The first objective in the paper will be to develop a method to compute the so-called delay margin, which is the difference between the system actual delay, τ , and the maximal delay limit, denoted τ_{\max} , beyond which the system becomes unstable. The underlying assumption here is that the increase in the value of τ pushes the system away from stability and closer to instability. Thus, the system is unstable if $\tau > \tau_{\max}$, and stable if $\tau < \tau_{\max}$. Furthermore, the system is stable independent of the delay if $\tau_{\max} = \infty$. τ_{\max} considered above is a function of the system parameters, or more precisely, the entries of the matrices \mathbf{A}_0 and \mathbf{A}_1 , whereas τ is independent of those parameters. Therefore, the task of computing the delay margin in the system can be viewed as the task of τ_{\max} . Section III presents the method to compute τ_{\max} .

D. Related Work

Investigating the effect of the delay on the stability of the retarded system dates back to several decade ago. Classical methods based on Bode or Nyquist plots are by far the preferred methods used to analyze the effect of the time-delay on the stability of digital speed controllers with loop time-delays [8] [9]. That is probably the case because they are easy to use and provide some insight if one seeks to investigate the stability of the system for a particular value of delay

τ . However, they are rather inconvenient if we either need to analyze the effect of a range of delay values or find the maximum loop time-delay beyond which the system becomes unstable.

During the last decade, other methods have been proposed to address this issue. Despite the fact that some accurate results have been reported, those methods are often computationally expensive for high-order systems because they map the original time-delay analysis to solving an equivalent LMI (Linear matrix Inequality) problem [12]–[18].

III. COMPUTING MAXIMAL STABLE DELAY IN LTI-RTDS, τ_{\max}

The objective in this section is to consider a system described by the LTI-RTDS described by (1) and ask the question: *what maximal value for the delay τ will turn the system to unstable system assuming that the system at $\tau = 0$ to be intrinsically stable?* The procedure described in this section has been presented in [10]. The theoretical background to this procedure has been presented in [10] [11], and a comparative study with other methodologies has been presented in [19]. A simplified and systematic application of this procedure is presented in the next subsection. We should also note that, in line of the assumption made about the system in (1), this method assumes that the delay-free system (i.e., $\tau = 0$) is stable by construction.

In general, the system is asymptotically stable for a given τ if, and only if, the roots of the characteristic polynomial obtained from

$$\text{CE}(s, \tau) := \det(s\mathbf{I} - \mathbf{A}_0 - \mathbf{A}_1 e^{-s\tau}) \quad (2)$$

or, alternatively, defined by

$$\text{CE}(s, \tau) = \sum_{k=0}^n p_k(s) e^{-sk\tau} \quad (3)$$

are all in the left-half plan of the complex s plan. $p_k(s)$ in the above equation is polynomial in s of degree $n - k$ with real coefficients.

The transcendental nature of $\text{CE}(s, \tau)$ produces an infinite number of roots, thereby making the task of analyzing the stability for given τ very complex, and finding τ_{\max} even more cumbersome.

A. Description of the Basic Procedure

In order to facilitate the description of finding τ_{\max} of a general LTI-RTDS, the following presentation will consider its application to an example LTI-RTDS given by

$$\mathbf{A}_0 = \begin{bmatrix} -2.0 & 0.0 \\ 0.0 & -0.9 \end{bmatrix}, \mathbf{A}_1 = \begin{bmatrix} -1.0 & 0.0 \\ -1.0 & -1.0 \end{bmatrix} \quad (4)$$

It is worth noting that for this example, the exact value of τ_{\max} is known *a priori* using an analytical argument as has been shown in [14]. This fact will be used to validate the result obtained from the procedure below with the exact solution. The procedure can be described as sequence of 6 steps summarized next.

- **Step 1.** Use the the Rekasius mapping to map $e^{-s\tau}$ as follows

$$e^{-s\tau} = \frac{1 - sT}{1 + sT}, T \in \mathbb{R} \quad (5)$$

where T is related to τ through the following relation

$$\tau = \frac{2}{\omega} (\tan^{-1}(\omega T) \mp l\pi), \quad l = 0, 1, 2, \dots \quad (6)$$

The above mapping transforms $\text{CE}(s, \tau)$ of (3) into a polynomial of degree $2n$ in s , whose coefficients are polynomials in T ,

$$\overline{\text{CE}}(s, T) = \sum_{j=0}^{2n} q_j(T) s^j \quad (7)$$

It is crucial to stress the fact that the Rekasius mapping is exact for $s = j\omega$, $\omega \in \mathbb{R}$, in the sense that $\overline{\text{CE}}(s, T) = \text{CE}(s, \tau) \forall s = j\omega$, where $j = \sqrt{-1}$.

In the example, taken for demonstration $n = 2$. This step would lead to the following polynomials

$$\begin{aligned} q_4(T) &= T^2 \\ q_3(T) &= 0.9T^2 + 2T \\ q_2(T) &= -0.1T^2 + 5.8T + 1 \\ q_1(T) &= 1.6T + 4.9 \\ q_0(T) &= 5.7 \end{aligned}$$

- **Step 2.** Form the Routh-Hurwitz array [20] for the s polynomial in (7)

$$\begin{array}{c|cccccc} s^{2n} & q_{2n}(T) & q_{2n-2}(T) & q_{2n-4}(T) & \cdots & q_0(T) \\ s^{2n-1} & q_{2n-1}(T) & q_{2n-3}(T) & \cdots & q_1(T) & 0 \\ s^{2n-2} & v_1^{(2n-2)}(T) & v_2^{(2n-2)}(T) & v_3^{(2n-2)}(T) & \cdots & 0 \\ s^{2n-3} & v_1^{(2n-3)}(T) & v_2^{(2n-3)}(T) & v_3^{(2n-3)}(T) & \cdots & 0 \\ \vdots & \vdots & & & & \\ s^2 & v_1^{(2)}(T) & v_2^{(2)}(T) & 0 & \cdots & 0 \\ s^1 & v_1^{(1)}(T) & 0 & \cdots & \cdots & 0 \end{array}$$

The application of this step to the particular example considered above will result in

$$\begin{aligned} v_1^{(2)}(T) &= \frac{-0.09T^4 + 3.42T^3 + 7.6T^2 + 2T}{0.9T^2 + 2T} \\ v_2^{(2)}(T) &= 5.7 \\ v_1^{(1)}(T) &= \frac{-0.144T^5 + 0.414T^4 + 8.4T^3 + 17.64T^2 + 9.8T}{-0.09T^4 + 3.42T^3 + 7.6T^2 + 2T} \end{aligned}$$

- **Step 3.** Compute the roots of $v_1^{(1)}(T) = 0$. This set of roots is referred to as T_{cr} , and for the current example are given by

$$T_{cr} = \{ -4.67, -2.22, -1.46, -1.0, 10.0 \}$$

- **Step 4.** Compute ω_{cr} using T_{cr} from

$$\omega_{cr} = \sqrt{\frac{v_2^{(2)}(T_{cr})}{v_1^{(2)}(T_{cr})}} \quad (8)$$

Note that T_{cr} (and consequently ω_{cr}) depends only on the state-space matrices \mathbf{A}_0 and \mathbf{A}_1 . Defining $\omega_{cr}^+ \subseteq \omega_{cr}$ as the subset of ω_{cr} with strictly positive values, and the corresponding T_{cr} values as T_{cr}^+ , use (6) to compute

$$\tau_{cr}^+ = \frac{2}{\omega_{cr}} \left(\tan^{-1}(\omega_{cr} T_{cr}) \mp l\pi \right), \quad l = 0, 1, 2, \dots \quad (9)$$

In the one-dimensional parameter space, τ , the above set represents the boundaries of the stable and unstable regions of delay of the LTI-RTDS.

- **Step 5.** Compute the Root Tendency (RT) using

$$RT = \text{sgn} \left[\Im \left(\frac{\sum_{k=0}^N a'_k e^{-sk\tau}}{\sum_{k=0}^N ka_k e^{-sk\tau}} \right) \right] \quad (10)$$

where $s = j\omega_{cr}^+$, $\tau = \tau_{cr}^+$, \Im denotes the imaginary part and “sgn” is the sign (± 1). RT represents the root transition direction crossing the imaginary axis to the unstable Right-Half Plan (RHP) ($RT = +1$) or to the stable Left-Half Plan (LHP) ($RT = -1$).

In the context of applying this procedure to the stability analysis of the BLDCM speed controller, it is typically the case that the delay-free system ($\tau = 0$) is stable by design. The question of finding the maximum delay of stable operation τ_{\max} then becomes finding the minimum member of the set τ_{cr}^+ such that $RT = +1$. This is the basis for the final step.

- **Step 6.** Compute τ_{\max} using

$$\tau_{\max} = \begin{cases} \min \tau_{cr}^+ & \text{if } \exists RT = +1 \\ \infty & \text{otherwise} \end{cases} \quad (11)$$

In the sense of (11), $\tau_{\max} = \infty$ implies that the LTI-RTDS is stable independent of the delay. The application of the last three steps to the example test case, yields

$$\omega_{cr}^+ = 0.4359, \quad RT = +1, \quad \tau_{\max} = 6.1726 \quad (12)$$

IV. DELAY-BASED MODELLING OF THE BLDCM CONTROL LOOP

This section turns the focus on the BLDC motor control loop. The ultimate objective in this section is to show how the closed-loop control of the BLDCM is properly cast as an LTI-RTDS of the form in (1).

To this end, the section first presents a brief background for the modeling of the BLDCM and the digital control loop. Section IV-A first describes a delay-free state-space model of the BLDCM motor. Section IV-B uses a closed-loop speed controller to derive a delay-based model for the transfer function of the set-point tracking and load disturbance rejection.

A. BLDCM State Space Model

Modeling of BLDC motor has been well studied in the literature, e.g. [1] [21] [22] [23]. Assuming that the BLDCM of Fig. 2 is symmetric in all three phases and that there is no

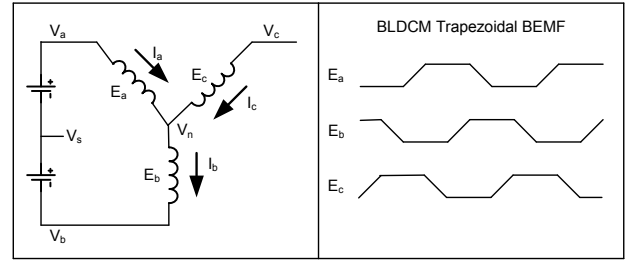


Fig. 2. BLDC Motor Electric Circuitry.

change in rotor reluctance with angle because of a non-salient rotor, its electrical circuitry model can be written as:

$$\begin{bmatrix} v_a \\ v_b \\ v_c \end{bmatrix} = \left(\begin{bmatrix} R_s & 0 & 0 \\ 0 & R_s & 0 \\ 0 & 0 & R_s \end{bmatrix} + \frac{d}{dt} \begin{bmatrix} L_s & 0 & 0 \\ 0 & L_s & 0 \\ 0 & 0 & L_s \end{bmatrix} \right) \begin{bmatrix} i_a \\ i_b \\ i_c \end{bmatrix} + \begin{bmatrix} e_a \\ e_b \\ e_c \end{bmatrix} \quad (13)$$

where v_a, v_b, v_c, i_a, i_b and i_c are the motor phase voltage and currents respectively, L and M are the winding self and mutual inductance, $L_s = L - M$ and e_a, e_b and e_c are the induced BEMF voltages. In a PMM, the BEMF is a function of the rotor position and can be written as $e(\theta) = \lambda\omega_r f(\theta)$, where λ represents the total flux linkage, ω_r is the motor shaft rotational speed. For a BLDCM, $f(\theta)$ is a trapezoidal function with peak values at $+1$ and -1 . For the sake of clarity, from now on we will omit the angle θ in the BEMF equation.

The generated electromagnetic torque is given by equation (14). If J is the rotor moment of inertia, B_m is the viscous friction coefficient and T_l is the load torque, then the mechanical model can be written as in (15).

$$T_e = \frac{e_a i_a + e_b i_b + e_c i_c}{\omega_r} \quad (14)$$

$$J \frac{d\omega_r}{dt} + B_m \omega_r = T_e - T_l \quad (15)$$

$$\frac{d\theta}{dt} = \omega_r \quad (16)$$

The state space model with $\mathbf{x}(t) = [i_a \ i_b \ i_c \ \omega_r]^T$ and $\mathbf{u}(t) = [v_a \ v_b \ v_c \ T_l]^T$ can be written as:

$$\begin{aligned} \frac{d\mathbf{x}(t)}{dt} &= \mathbf{A}\mathbf{x}(t) + \mathbf{B}\mathbf{u}(t) \\ \mathbf{y}(t) &= \mathbf{C}\mathbf{x}(t) \end{aligned} \quad (17)$$

$$\mathbf{A} = \begin{bmatrix} -R/L & 0 & 0 & \lambda f_a(\theta)/L & 0 \\ 0 & -R/L & 0 & \lambda f_b(\theta)/L & 0 \\ 0 & 0 & -R/L & \lambda f_c(\theta)/L & 0 \\ \lambda f_a(\theta)/J & \lambda f_b(\theta)/J & \lambda f_c(\theta)/J & -B_m/J & 0 \end{bmatrix}$$

$$\mathbf{B} = \begin{bmatrix} 1/L & 0 & 0 & 0 \\ 0 & 1/L & 0 & 0 \\ 0 & 0 & 1/L & 0 \\ 0 & 0 & 0 & -1/J \end{bmatrix}$$

Assuming the BLDC motor is phase-balanced and wye-connected then $i_a + i_b + i_c = 0$ and $v_s = \sum_{i=a}^c v_i - \sum_{i=a}^c e_i$. Note that the motor can be modeled by just two currents as the third current is dependent of the other two. From the previous

equations, we can derive the BLDCM non linear state space model with state variables i_a , i_b and ω_r , given by:

$$\mathbf{A} = \begin{bmatrix} -R/L & 0 & \lambda/3L(2f_a - f_b - f_c) \\ 0 & -R/L & \lambda/3L(2f_b - f_a - f_c) \\ \lambda/2J(f_a - f_c) & \lambda/2J(f_b - f_c) & -B_m/J \end{bmatrix}$$

$$\mathbf{B} = \frac{1}{3L} \begin{bmatrix} 2 & -1 & -1 & 0 \\ -1 & 2 & -1 & 0 \\ 0 & 0 & 0 & -3L/J \end{bmatrix}$$

where the state variable $\mathbf{x}(t) \in \mathbb{R}^3$ is given by $\mathbf{x}(t) = [i_a \ i_b \ \omega_r]^T$ and the input vector $\mathbf{u}(t) \in \mathbb{R}^4$ is given by $\mathbf{u}(t) = [v_a \ v_b \ v_c \ T_l]^T$. $\mathbf{A} \in \mathbb{R}^{3 \times 3}$, $\mathbf{B} \in \mathbb{R}^{3 \times 4}$ and $\mathbf{C} = \mathbf{I} \in \mathbb{R}^{3 \times 3}$ are the matrices describing the dynamics of the BLDCM continuous-time model (CTM). We can further simplify the model in (17) to make it easier to analyze the BLDCM dynamical behavior as a function of its mechanical and electrical parameters. In a BLDCM, at any time there are only two phases being driven while the third phase is open. Assuming that $B_m \ll 0$ such that $B_m R \approx 0$ and $B_m L \approx 0$, and that phases a and b are driven by a voltage source v_a and v_b respectively, then $i_c = 0$ and $i_a = -i_b$. Therefore, the model in (17), with $k_e = 2\lambda$, $\mathbf{x}(t) = [i_a \ \omega_r]^T$, $\mathbf{u}(t) = [(v_a - v_b) \ T_l]^T$, can be rewritten as:

$$\begin{aligned} \frac{d\mathbf{x}(t)}{dt} &= \mathbf{A}_{2 \times 2} \mathbf{x}(t) + \mathbf{B}_{2 \times 2} \mathbf{u}(t) \\ \mathbf{y}(t) &= \mathbf{C}_{2 \times 2} \mathbf{x}(t) \end{aligned} \quad (18)$$

$$\mathbf{A}_{2 \times 2} = \begin{bmatrix} -R/L & -k_e/L \\ k_e/J & -B_m/J \end{bmatrix}$$

$$\mathbf{B}_{2 \times 2} = \begin{bmatrix} 1/L & 0 \\ 0 & -1/J \end{bmatrix}$$

B. BLDCM Speed Controller With Loop Delays

This section derives a closed-form for the BLDCM speed controller that includes the control loop delays. Figure 3 presents the linearized model of a BLDCM speed controller showing various sources of delay in the control loop. As the figure shows, there are three sources of delay in the control loop. Those are

- 1) The delay introduced by the Hall sensor, τ_h , can be estimated using the rotational speed ω_r in *rad/s* as follows

$$\tau_h = \frac{2\pi}{6\omega_r} \quad (19)$$

- 2) The delay arising from the discretization of the PI controller and the Low-Pass Filter (LPF), with each introducing a time delay τ . This delay is equivalent to the sampling time used in the discretization of the PI controller and LPF CTM transfer functions.

Next, we consider the transfer function of each component in the control loop. First the PI controller transfer function is given by

$$H_p(s) = \frac{V_p(s)}{\Omega_e(s)} = k_p \frac{\tau_{iw}s + 1}{\tau_{iw}s} e^{-s\tau}, \quad (20)$$

$$\tau_{iw} = \frac{k_p}{k_i} \quad (21)$$

where k_p is the proportional gain, and k_i is the integral gain.

The Pulse-Width-Modulator (PWM) component has the transfer function, $H_{\text{PWM}}(s)$, which is given by,

$$H_{\text{PWM}}(s) = \frac{V_a(s)}{V_p(s)} = \frac{V_{dc}}{\tau_{\text{pwm}}s + 1}, \quad (22)$$

where $\tau_{\text{pwm}} = 0.5f_{\text{pwm}}$, and f_{pwm} is the modulation frequency. Typically, f_{pwm} is much faster than the sampling frequency ($f_s = 1/\tau$). This allows $H_{\text{PWM}}(s)$ to be reasonably approximated using $H_{\text{PWM}}(s) \approx V_{dc}$.

The motor electrical transfer function between the phase current and the terminal voltage is given by

$$H_{\text{elec}}(s) = \frac{I_a(s)}{V(s)} = \frac{1/R}{\tau_e s + 1}, \quad (23)$$

where $\tau_e = \frac{L}{R}$, while its mechanical transfer function, that is, the one between rotational speed and driving torque is given by

$$H_{\text{mech}}(s) = \frac{\Omega_r(s)}{T_e(s) - T_l(s)} = \frac{1/B_m}{\tau_m s + 1}, \quad (24)$$

where $\tau_m = \frac{J}{B_m}$.

The transfer function between the terminal voltage $V(s) = V_a(s) - V_b(s)$ and the shaft rotational speed $\Omega_r(s)$, denoted by $H_m(s)$, can be obtained from (18) using the system transfer function $\mathbf{H}(s) = \mathbf{C}_{2 \times 2} (s\mathbf{I} - \mathbf{A}_{2 \times 2})^{-1} \mathbf{B}_{2 \times 2}$ and setting $T_l = 0$ (assuming that $B_m \approx 0$), as shown next,

$$H_m(s) = \frac{\Omega_r(s)}{V(s)} = \frac{1/k_e}{\frac{RJ}{k_e^2} \frac{L}{R} s^2 + \frac{RJ}{k_e^2} s + 1} \quad (25)$$

Defining the electrical and mechanical time constants as $\tau_{\text{elec}} = L/R$ and $\tau_{\text{mech}} = RJ/k_e^2$, respectively, we can rewrite (25) as

$$H_m(s) = \frac{1/k_e}{\tau_{\text{mech}}\tau_{\text{elec}}s^2 + \tau_{\text{mech}}s + 1} \quad (26)$$

Finally, the LPF has the transfer function

$$H_{\text{LPF}}(s) = \frac{\Omega_f(s)}{\Omega_s(s)} = \frac{k_f}{\tau_f s + 1} e^{-s\tau} \quad (27)$$

From control systems theory we can easily see that the set-point tracking transfer function $H_{\text{SP}}(s)$ assuming the load torque input $T_l = 0$ is given by,

$$\begin{aligned} H_{\text{SP}}(s) &= \frac{\Omega_r(s)}{\Omega_{\text{ref}}(s)} \\ &= H_p(s) H_{\text{PWM}}(s) H_m(s) H_f(s) e^{-s\tau} \left(1 + H_p(s) \right. \\ &\quad \left. \times H_{\text{PWM}}(s) H_m H_{\text{LPF}}(s) e^{-s(2\tau + \tau_h)} \right)^{-1} \end{aligned} \quad (28)$$

where $H_f(s)$ is the transfer function of the input speed profiler.

Similarly, taking the rotational reference speed $\omega_{\text{ref}} = 0$ enables deriving the load disturbance transfer function, $H_{\text{load}}(s)$, as follows,

$$\begin{aligned} H_{\text{load}}(s) &= \frac{\Omega_r(s)}{T_l(s)} \\ &= H_{\text{mech}}(s) \left(1 + k_e H_{\text{elec}}(s) H_{\text{mech}}(s) \right. \\ &\quad \left. + H_p(s) H_{\text{PWM}}(s) H_{\text{LPF}}(s) H_{\text{elec}}(s) \right. \\ &\quad \left. \times H_{\text{mech}}(s) e^{-s(2\tau + \tau_h)} \right)^{-1} \end{aligned} \quad (29)$$

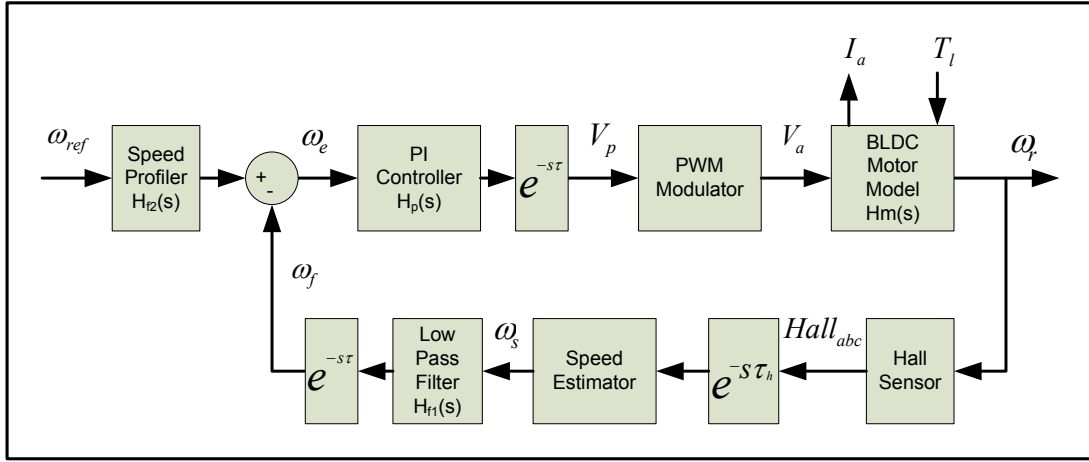


Fig. 3. BLDC motor speed controller with sources of delay.

The continuous-time delay of the Hall sensor τ_h can only be seen between two sampling times τ . Therefore, its contribution to the loop delay is given by $\sup(\frac{\tau_h}{\tau})$. Looking at equations (28) and (29), we can notice that, in both transfer functions, all delay contributions are lumped together in the total time-delay

$$\tau_{\text{total}} = m\tau \quad (30)$$

with

$$m = 2 + \sup(\frac{\tau_h}{\tau}). \quad (31)$$

C. Summary and Discussion

The preceding developments in this section aimed at taking into account all the sources of delays induced by the various modules in the control loop of the BLDCM and arriving to an LTI-RTDS of the form (1). This was accomplished by deriving the set-point tracking and load-disturbance rejection transfer functions, respectively, in (28) and (29). Converting those transfer functions into the state-space LTI-RTDS format of (1) is straightforward but not needed at this point, since the current goal is to use the method outlined in Section III, which proceeds starting from the characteristic polynomial in (3). The next step is therefore to extract the characteristic polynomial corresponding to the transfer functions in (28) or (29). It is to be noted that τ_{total} in those transfer functions represents the actual delay of the system, which was labelled simply as τ in Section III.

The next section will pursue the quest of computing τ_{max} for a system whose transfer functions are given by (28) and (29).

V. EFFECT OF DELAY ON THE STABILITY

This section aims at applying the method outlined in Section III to compute τ_{max} of the delay-based model of the BLDCM developed in Section IV.

As a first step towards towards this goal, we first note that the denominators of the above derived transfer functions (28) and (29) are quasi-polynomials in s , which take the same form as the characteristic polynomial of the LTI-RTDS in (3). Therefore, the steps described in Section III to determine the

maximum delay of stable operation of the LTI-RTDS can be employed, with slight modifications, to determine τ_{max} : the maximum allowable delay for τ_{total} under stable operation. Denoting the denominator quasi-polynomials in (28) and (29) by $\text{CE}_{\text{SP}}(s, \tau_{\text{total}})$, and $\text{CE}_{\text{load}}(s, \tau_{\text{total}})$ while using the delay τ_{total} defined in (30) and (31), we get

$$\text{CE}_{\text{SP}}(s, \tau_{\text{total}})(s) = k_s(\tau_{iw}s + 1)e^{-s\tau_{\text{total}}} + \tau_{iw}s(\tau_l s + 1)(\tau_{f1}s + 1) \quad (32)$$

$$\text{CE}_{\text{load}}(s, \tau_{\text{total}})(s) = k_l(s\tau_{iw} + 1)e^{-s\tau_{\text{total}}} + sk_m(s\tau_{f1} + 1) + sk_n(s\tau_e + 1)(s\tau_m + 1)(s\tau_{f1} + 1) \quad (33)$$

where $k_s = \frac{k_p V_{dc}}{k_e}$, $k_l = \frac{k_p k_e k_{f1} V_{dc}}{R}$, $k_m = \tau_{iw} \frac{k_e^2}{R}$ and $k_n = B_m \tau_{iw}$.

Next, we proceed with Step 1 in the method described in Section III to find τ_{max} . We will limit the following analysis to $\text{CE}_{\text{load}}(s, \tau_{\text{total}})(s)$ noting that $\text{CE}_{\text{SP}}(s, \tau_{\text{total}})$ can be treated in a like manner.

Using the Rekasius mapping (5) in (33) results in transforming (33) into,

$$\overline{\text{CE}}_{\text{load}}(s, T) = \sum_{i=0}^5 q_i(T) s^i \quad (34)$$

where,

$$\begin{aligned} q_5(T) &= k_n \tau_e \tau_m \tau_{f1} T \\ q_4(T) &= k_n \tau_e \tau_m \tau_{f1} + (k_n \tau_e \tau_m + k_n \tau_e \tau_{f1} + k_n \tau_m \tau_{f1}) T \\ q_3(T) &= k_m \tau_e \tau_m + k_n \tau_e \tau_{f1} + k_n \tau_m \tau_{f1} \\ &\quad + (k_m \tau_{f1} + k_n \tau_e + k_n \tau_m + k_n \tau_{f1}) T \\ q_2(T) &= k_m \tau_{f1} + k_n \tau_e + k_n \tau_m + k_n \tau_{f1} \\ &\quad + (k_m + k_n - k_l \tau_{iw}) T \\ q_1(T) &= k_l \tau_{iw} + k_m + k_n - k_e T, \\ q_0(T) &= k_l \end{aligned}$$

The rest of steps in Section III, starting with step 2, can be automated and implemented in a Matlab script culminating with τ_{max} .

At this point, few remarks are worthy of note in order to highlight the significance of τ_{\max} computed by the above procedure.

- Given that the delay-free speed controller ($\tau_{\text{total}} = 0$) is nominally stable by design, it follows that τ_{\max} computed using the above steps represents an upper bound on τ_{total} beyond which the system becomes unstable. In other words, τ_{\max} is the maximum delay that the closed-loop system can tolerate before the roots of its characteristic quasi-polynomial cross to the RHP (rendering the system unstable) as τ_{total} is increased above 0.
- The value for τ_{\max} calculated by the above steps depends solely on the BLDC motor and speed controller parameters, and is independent of the motor operating conditions, e.g. the rotational speed of the motor. This fact makes the condition $\tau_{\text{total}} < \tau_{\max}$ a necessary condition for the stability that is given *a priori* independent of the operating conditions.
- The value of τ_{total} (which depends on the actual operating conditions of the motor) and its proximity to τ_{\max} can be used to serve as a measure for the stability of the speed controller. For example, the further τ_{total} is from τ_{\max} the closer the system is to its stable delay-free condition.
- Given a nominal set of operating conditions, a controller design with bigger τ_{\max} is more robust to changes in the closed-loop delay.

VI. EFFECT OF CONTROLLER PARAMETERS ON THE STABILITY

The goal in this section is employ the procedure developed in Section V for computing τ_{\max} as a lens, so to speak, that enables viewing the various commonly used PI tuning rules from a totally different angle. More specifically, we examine the impact of the choice of the controller parameters on τ_{\max} . This task will be carried out in several steps.

- In the first step, we will consider some of the widely used PI tuning rules, and examine their choices for the PI controller parameters (k_p and k_i) through the lens of their impact on τ_{\max} . This step is given in Section VI-A.
- Next, we will let those parameters vary continuously, within reasonable ranges, and plot, in Section VI-B, the corresponding values for τ_{\max} , where we find new insights that, to the best of the authors' knowledge, remained hitherto unknown.
- Finally, in Section VI-B2, we study the effect of the LPF cutoff frequency, ω_f , on τ_{\max} .

Before proceeding further, we need to present the operating conditions and the basic setup established for this study.

The motor chosen to conduct this study is the Beijing BL3056 which comes with the TI Stellaris RDK-BLDC design kit (which we refer to as the TI controller). The main motor parameters are given in Table I, and the TI controller parameters, for the LPF and PI controller, are given in tables II and III respectively. The reader is referred to [24] for additional details. We also considered the load disturbance rejection response, through its quasi-polynomial, to calculate τ_{\max} . The control input is the disturbance torque in N.m and the output

is the BLDCM shaft angular speed in *rad/s*. Finally, the total loop delay τ_{total} was set to 3.7ms (equivalent to a rotational speed of 6000 RPM and $\tau = 1\text{ms}$).

TABLE I
BEIJING BLDCM BL3056 PARAMETERS.

R Ω	L mH	J g.cm ²	k_t N.A/m	k_e V/RPM	τ_{elec} ms	τ_{mech} ms
2.3	0.56	16.0	0.0223	0.00234	0.24	7.4

TABLE II
PARAMETERS OF TI STELLARIS RDK-BLDC SPEED CONTROLLER

k_f	τ_f (ms)	ω_f (rad/s)
1.0	3.48	287.7

A. Effect of PI Controller Tuning Rules on τ_{\max}

We analyze in this section the relationship between τ_{\max} and various popular PI controller tuning rules including Ziegler-Nichols (Z-N), Chien-Hrones-Reswick (CHR) and the methods based on the integral error criteria (Integral of Square Error - ISE, Integral of Absolute Value Error - IAE, Integral Time Squared Error - ISTE and Integral Time Absolute Error - ITAE) [25].

Table III shows the values of k_p and k_i , and the corresponding values for τ_{\max} , obtained for each one of those tuning rules, with the values of the LPF set to those given in Table II. Note that several tuning rules of those listed in Table III have two different values for both k_p and k_i . Those two sets of values correspond to whether the tuning rule is being optimized for load disturbance rejection or set point tracking responses, marked by † or ‡, respectively. The table also shows, in the first row, the values for k_p and k_i selected by the TI controller, as well as the response obtained by the custom rule of the TI controller.

To visualize the performance obtained from each of the above tuning rules, Figs. 4 and 5 present the transient response of the system. Fig. 4 groups the result - corresponding to tuning rules optimized for set point tracking responses, whereas Fig. 5 shows the results obtained for the rules optimized for load disturbance rejection.

The foremost remarks seen from the above results can be summarized by the following points.

- The tuning rules optimized for load disturbance rejection produce behaviours more robust to delays compared to those optimized for set point tracking response. It should be observed too that the former set results in larger values for τ_{\max} than the latter set.
- The TI commercial controller tuning values of Table II result in an excessively large τ_{\max} compared to the other methods. Hence, the TI controller should be very robust regarding the loop delay τ_{total} . However, this highly desirable property comes at the expense of a very sluggish transient response as shown in Fig. 5.

TABLE III
EFFECT OF VARIOUS TUNING RULE ON τ_{max}

Tuning Rule	Parameters values			
	$k_p \times 10^{-3}$	$k_i \times 10^{-6}$	$\tau_{iw} = \frac{k_p}{k_i}$ (ms)	τ_{max} (ms)
TI *	0.122	0.366	333	4274
CHR †	1.024	65.43	15.65	12.8
ISE †	0.669	20.10	33.28	18.9
ISTE †	0.527	26.87	19.61	16.7
Z-N ‡	1.536	117.9	13.03	5.2
CHR ‡	1.024	142.5	7.188	8.3
ISE ‡	1.566	132.0	11.87	4.9
ISTE ‡	1.158	134.3	8.624	7.5
IAE ‡	1.160	135.9	8.532	7.4
ITAE ‡	1.472	135.9	10.83	5.3

* The tuning parameters set by the TI Stellaris kit.
 † Tuning rules for load disturbance rejection response.
 ‡ Tuning rules for set-point tracking response.

The above remarks are indeed in line with the rationale behind the proposed method, which is premised on the notion that design methodologies that yield larger values for τ_{max} produce more robust behavior that is less sensitive to loop delays.

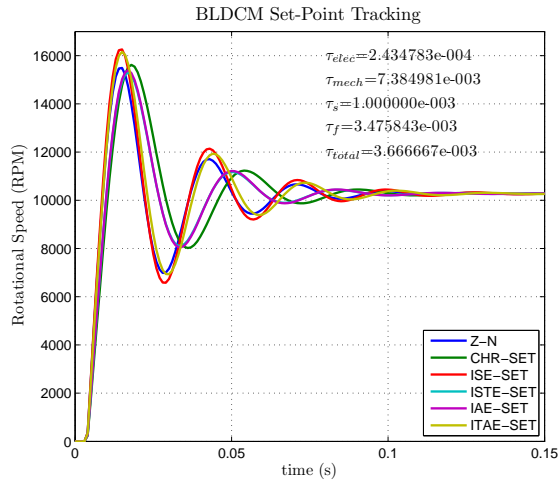


Fig. 4. PI controller Set-Point Tracking Response for Various Tuning Rules.

B. Effect of Widely Varying k_p and k_i on τ_{max}

In this section we further analyze the impact of the speed controller design choices on the value of τ_{max} , through sweeping the values of k_p and k_i , for some selected values of ω_f , and calculating τ_{max} using the method proposed in section V.

1) *High ω_f* : In the first set of experiments, we minimize the effect of the LPF by setting ω_f to be one order of magnitude bigger than the value in table II ($\omega_f = 2877 \text{ rad/s}$). Fig. 6 shows τ_{max} corresponding to sweeping k_p , in a wide range of values, while setting τ_{iw} (by adjusting k_i) to values ranging from $0.25\tau_{mech}$ to $32\tau_{mech}$.

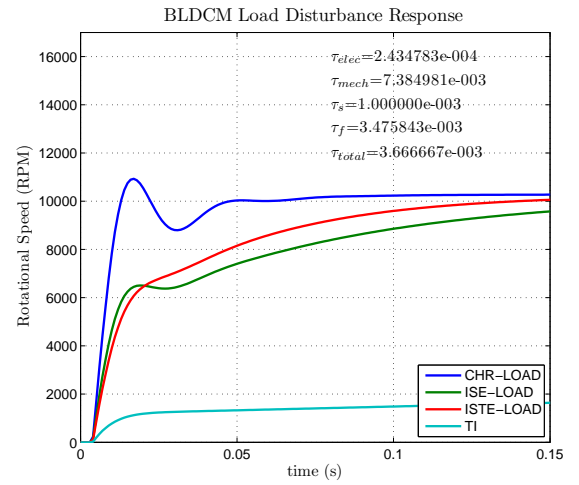


Fig. 5. PI controller Load Disturbance Response for Various Tuning Rules.

It is important to note here that at high k_p values (about 1.8×10^{-3}), the smaller values for τ_{max} suggest that the controller becomes more sensitive to delays in the control loop. We can also see that changes in τ_{iw} do not significantly affect the maximum loop time-delay τ_{max} , in this range. Consequently, around this range, k_p dominates the controller behavior and robustness to delays.

On the other hand, at lower values of k_p , τ_{max} can be many orders of magnitude bigger than its value at high k_p . Consequently, the controller is much more robust to delays at low k_p . It is important to notice that at this range, for the same k_p , τ_{max} can vary by more than two orders of magnitude depending on the value of τ_{iw} . Therefore, at this range, the controller designer has two degrees of freedom (k_p and τ_{iw}) to design a controller with a proper trade-off between speed and robustness to delays.

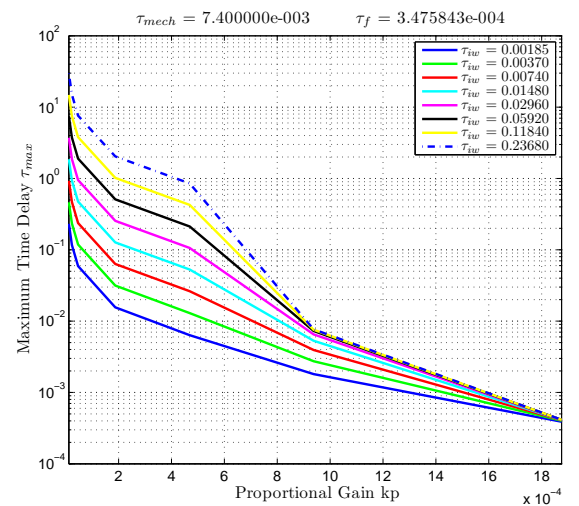


Fig. 6. Effect of PI controller on τ_{max} ($\omega_f = 2877 \text{ rad/s}$).

2) *Medium and small ω_f* : Here we analyze the effect of the LPF cutoff frequency ω_f on the robustness of the speed controller to time-delays. First, we set ω_f to its TI controller value of table II and repeat the calculations of section VI-B.

As we can see in Fig. 7, at this cutoff frequency and at high k_p , changes in τ_{iw} affect τ_{max} more than for the previous case when ω_f was large. On the other hand, at low k_p , the smaller ω_f causes almost no change on τ_{max} .

Decreasing ω_f further to 10% the value in table II causes τ_{max} to become even more sensitive to τ_{iw} at high k_p , as shown in figure 8. Actually, τ_{max} becomes significantly bigger indicating that the controller becomes less sensitive to delays in the control loop with smaller LPF cutoff frequencies. However, τ_{max} values at low k_p remain almost unchanged.

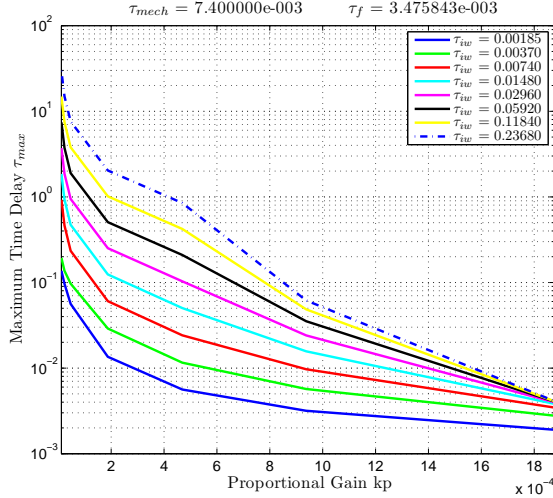


Fig. 7. Effect of PI controller on τ_{max} ($\omega_f = 287.7$ rad/s).

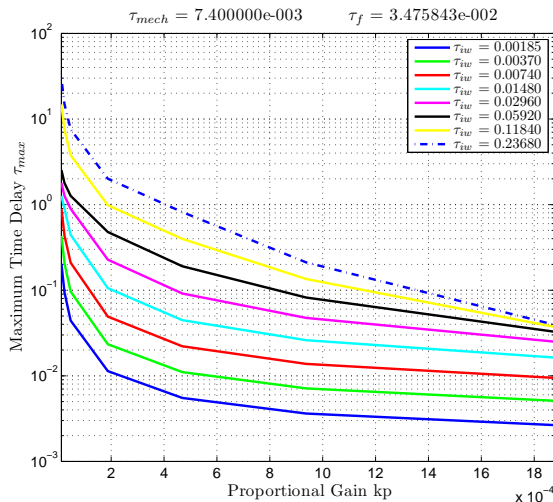


Fig. 8. Effect of PI controller on τ_{max} ($\omega_f = 28.77$ rad/s).

VII. EXPERIMENTAL RESULTS

This section demonstrates experimentally the advantage of the proposed stability analysis under different operating conditions. The approach followed in the presentation of this section is to juxtapose the stability criteria established by the proposed method, namely, the requirement that $\tau_{total} < \tau_{max}$ for stable operation, and the classical stability conditions based

on the phase and gain margins obtained through the Nyquist plot. This process is carried out for speed controllers designed by a subset of the tuning rules given in Table III for different operating conditions of the rotational speed ω_r .

It should be noted, however, that the criteria based on the classical methods need to be repeated for all desired operating conditions, whereas in the proposed method τ_{max} is independent of the operating conditions and therefore is more convenient to use.

This section presents both simulation and experimental results whose setup is described briefly in the next subsection.

A. Simulation and Experimental Setup

The transient time-domain simulation results were obtained by constructing a Simulink model for the BLDC motor and the PI controller and LPF. Those transient simulations show the simulation results for the continuous-time model (CTM) with and without delay and for the discrete-time model (DTM) with delay. The experimental results were obtained using a Stellaris BL3056 BLDC motor control reference design kit (RDK-BLDC) and a Xilinx University program Virtex II Pro Development kit. The generator stator was connected to various resistive loads through an array of electronically controlled power switches. This setup allowed us to quickly connect and disconnect loads to the generator creating accurate transient torque scenarios with good accuracy and repeatability.

B. Description of the Experiments

The rows in Table IV summarize the results obtained for the TI speed controller, as well as three of the tuning rules given earlier in Table III under two operating conditions of the rotational speeds $\omega_r = 6000$ and 1000 RPM, which are about 75% and 10% of the BL3056 rated speed, respectively. Those values of ω_r correspond to values of τ_h of 1.67 and 10 ms, respectively. Table IV also provides the Phase Margin (PM) obtained in each tuning rule and under the two operating conditions. The table illustrates the agreement between the marginal stability criteria in the classical method (PM $> 0^\circ$) and the stability criteria in the proposed method ($\tau_{total} < \tau_{max}$). However, the classical method based on the PM does not provide the amount of delay in τ_{total} before the system becomes unstable.

1) *Stability Characteristics of the TI Controller:* Figs. 9- 11 show the Nyquist plots and the transient responses for the TI controller under three rotational speeds $\omega_r = 1000, 5$ and 3 RPM, respectively.

For $\omega_r = 1000$ RPM, $\tau_h \approx 1$ ms. Therefore, $\tau_{total} \ll \tau_{max}$, implying that the TI controller should be very stable with no oscillations. This fact is confirmed by the transient response shown in Fig. 9 which shows the three transient responses (CTM with and without delay, and DTM with delay) to coincide perfectly. However, this desired stability response comes at the expense of a very sluggish behaviour, as shown by the measured response in Figs. 12 and 13, which show TI controller transient response when the reference speed change from 1000 RPM to 6000 RPM (no load condition) and

TABLE IV
STABILITY CONDITIONS UNDER TWO DIFFERENT OPERATING CONDITIONS

Tuning Method	τ_{max}	Operating Condition ω_r, τ_{total}			
		6000 RPM, $\tau_{total} \approx 3.7$ ms		1000 RPM, $\tau_{total} = 12.0$ ms	
		$\tau_{total} < \tau_{max}$	PM	$\tau_{total} < \tau_{max}$	PM
TI	4274	TRUE	82.7	TRUE	82.1
CHR [†]	12.8	TRUE	42.4	TRUE	9.87
ISE [†]	18.9	TRUE	59.9	TRUE	46.6
Z-N	5.2	TRUE	24.8	FALSE	-35.2

[†] Tuning rules for optimized load disturbance rejection response.

the load torque change from 0 mN · m to 27.8 mN · m, respectively.

On the other hand, for $\omega_r = 5$ RPM we have a $\tau_{total} = 2$, which is slightly less than half of τ_{max} . As Fig. 10, at this speed the system starts approaching the stability boundary as evidenced by the oscillations in the transient responses.

Finally, at $\omega_r = 3$ RPM, $\tau_{total} = 3.34$, approaching the τ_{max} limit of stable operation. As shown in Fig. 11 the response becomes increasingly oscillatory.

2) Stability of Conservative and Agressive Tuning Rules:

Figs. 9, 10 and 11 show the Nyquist plot and the step response of the TI controller at rotational speeds ω_r of 1000 RPM, 5 RPM and 3 RPM respectively. At 1000 RPM ($\tau_h = 10ms$), we have $\tau_{total} \ll \tau_{max}$ which implies the TI controller should be stable and show low sensitivity to ω_r . These results are confirmed by the similar gain margin for 1000 RPM and 6000 RPM in table IV and no sign of oscillatory behavior in figure 9. The small τ_{total} and τ_h , compared to τ_{max} , cause the three graphics coincide in figure 9.

approaches τ_{max} , the step response oscillatory behavior shown in figure 11 has significantly increased.

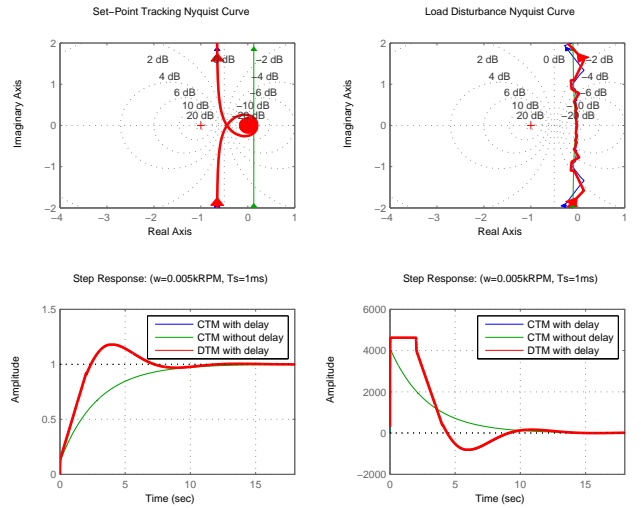


Fig. 10. Delay Effect Using TI controller tuning values at $\omega_r = 5$ RPM.

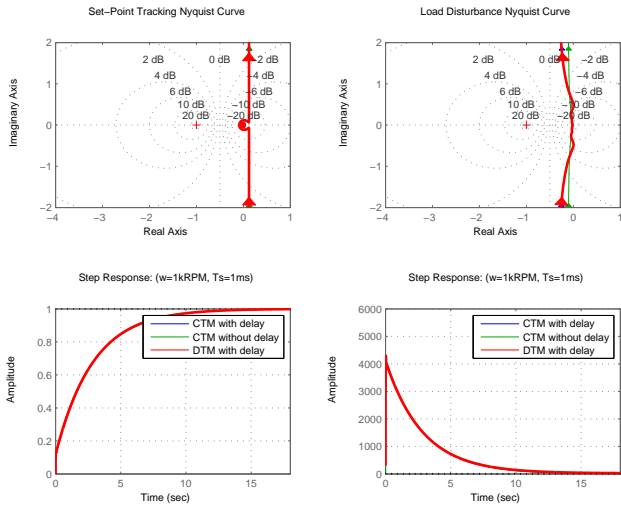


Fig. 9. Delay Effect Using TI controller tuning values at $\omega_r = 1$ kRPM.

At $\omega_r = 5$ RPM ($\tau_{total} \approx 2ms$), τ_{total} is just a little less than half of τ_{max} . It is straightforward to see in figure 10 that the system starts approaching the stability boundary as evidenced by the oscillation on its step response. Beyond $\tau_{total} = 0.5 \cdot \tau_{max}$ it quickly approaches instability becoming fully unstable at $\tau_{total} = \tau_{max}$. At $\omega_r = 3$ RPM ($\tau_{total} = 3.34ms$), as τ_{total}

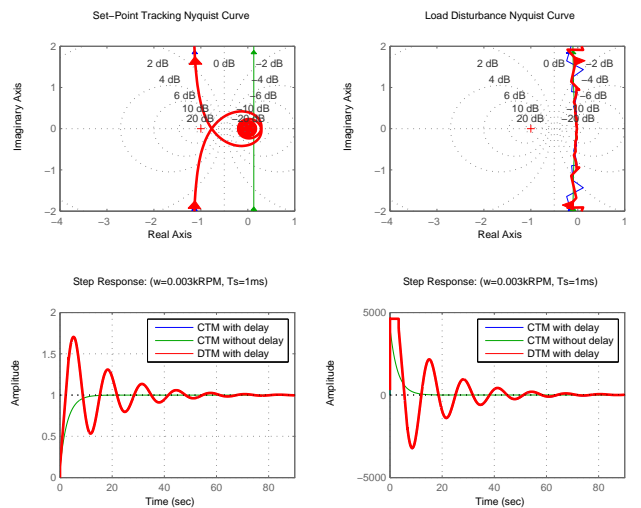


Fig. 11. Delay Effect Using TI controller tuning values at $\omega_r = 3$ RPM.

Figures 12 and 13 show the It confirms the sluggish response of the TI controller to set-point tracking and load disturbance rejection responses.

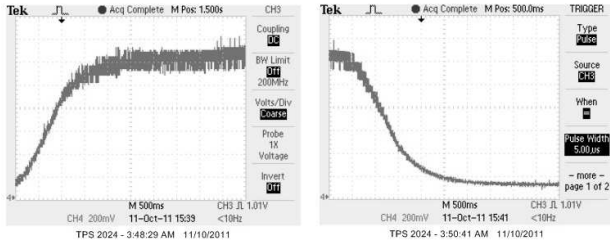


Fig. 12. Speed transient from 1000 to 6000 RPM at no load.

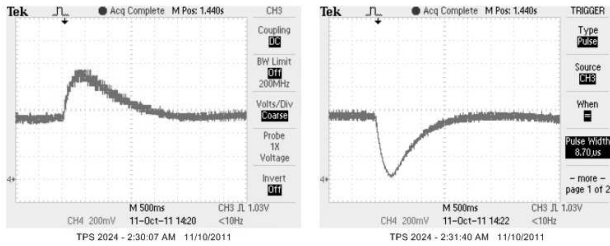


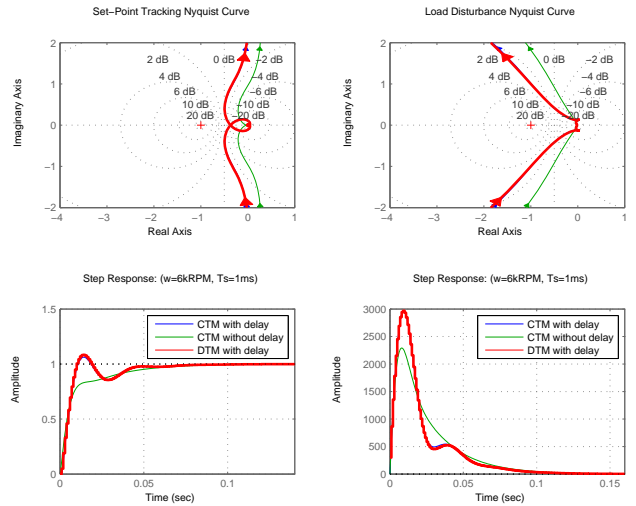
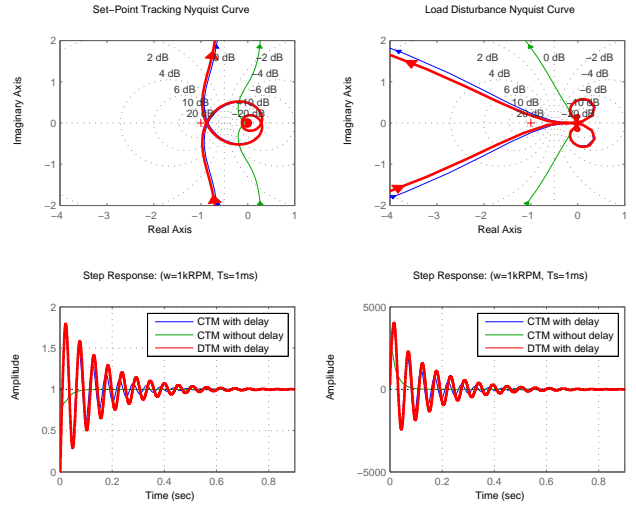
Fig. 13. Torque transient test at 3000 RPM (0 - 27.8 m NM - 0).

In summary, the TI controller k_p and k_i values produce a controller capable of handling total loop time-delays of up to 2.0s. However, its robustness to loop time-delay comes at the expense of very slow dynamical responses. It is highly desirable to tune PI controllers to robustness and stability but still be able to achieve fast dynamical response.

3) *Stability of Fast And Stable Tuning Rules:* The objective of this section is to study the stability conditions of the remaining three rules tuned to fast response and how τ_{\max} correlates to them. Here we compare two tuning rules: CHR-load and ISE-load. The popular Ziegler-Nichols (Z-N) method is well known for producing oscillatory responses. Looking at the gain and phase margins of table IV, we can see the Z-N tuning values result in a τ_{total} that is too close to τ_{\max} and will not be considered here.

Among the classical methods tested, the CHR, for optimized load disturbance rejection, of Figs. 14 and 15 provided the best compromise between smooth and fast response at $\omega_r = 6000 \text{ RPM}$. At this speed, τ_{total} is only 30% of τ_{\max} ($\tau_{\max} = 12.8 \text{ ms}$) with a rise time of about 10ms and overshoot of 30%. For the same BLDCM and LPF, the CHR tuning, also for optimized load disturbance rejection, is about 700 faster than the TI controller. As we increase τ_h (by decreasing ω_r to 1000 RPM), we have $\tau_{\text{total}} \approx \tau_{\max}$ causing the system to behave with a significant oscillatory step response at $\omega_r = 1000 \text{ RPM}$.

With a high τ_{\max} value of 18.9ms, the ISE tuning method, optimized for load disturbance rejection, is the most stable and robust to time-delays among all methods tested. At $\omega_r = 6000 \text{ RPM}$, its τ_{total} is less than 20% of τ_{\max} resulting in a step response with no overshoot as shown in Fig. 16. This smoother response comes at the expense of a rise time that is 12 times longer compared to CHR (load) tuning (120ms for ISE (load) compared to 10ms of CHR (load)). With a 48% overshoot at $\omega_r = 1000 \text{ RPM}$ ($\tau_{\text{total}} \approx 0.6 \cdot \tau_{\max}$), the ISE-

Fig. 14. Delay Effect Using CHR-load tuning values at $\omega_r = 6 \text{ kRPM}$.Fig. 15. Delay Effect Using CHR-load tuning values at $\omega_r = 1 \text{ kRPM}$.

load step response in figure 17 starts to show an oscillatory step response.

VIII. CONCLUSIONS

This work presented an effective algebraic technique to analyze the asymptotic stability of a BLDCM speed controller with strong time-delays in the control loop. We have shown that given a BLDCM, the k_p and k_i PI controller parameters, and the LPF cutoff frequency ω_{f1} , there is a maximum time-delay τ_{\max} beyond which the total total closed loop time-delay τ_{total} causes the system to become unstable and presented a method to calculate τ_{\max} . Experimental results confirm the method is more accurate and less conservative than previously reported ones.

Based on the mathematical definitions of τ_{\max} and τ_{total} , and confirmed by experimental results, we suggest that the ratio $\tau_{\max}/\tau_{\text{total}}$ can be used as a metric to assess the controller robustness to additional delays in the control loop. Different than the classical methods which require one plot for each rational speed, τ_{\max} depends only on the controller parameters.

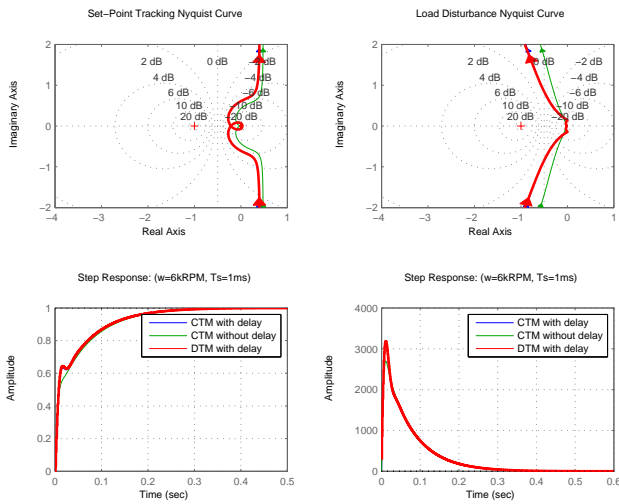


Fig. 16. Delay Effect Using ISE-load tuning values at $\omega_r = 6 \text{ krPM}$.

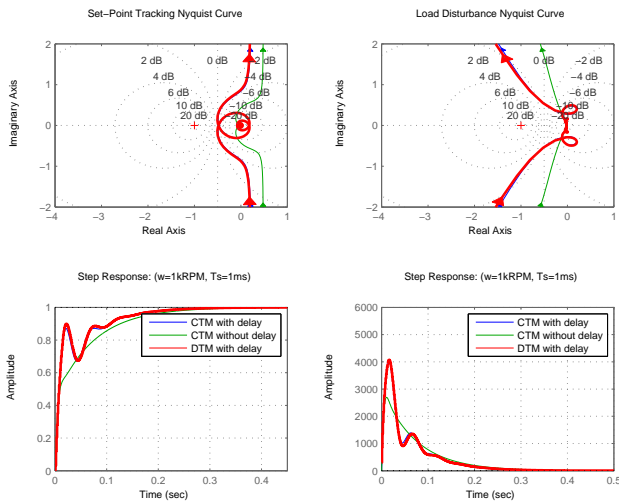


Fig. 17. Delay Effect Using ISE-load tuning values at $\omega_r = 1 \text{ krPM}$.

Hence, it does not change with operating conditions making the proposed method much simpler to use than the classical ones. Finally, it is worth noticing the method proposed here can be easily extended to other types of speed estimators (such as the back EMF methods) as well as to analyze the stability of the set-point tracking response.

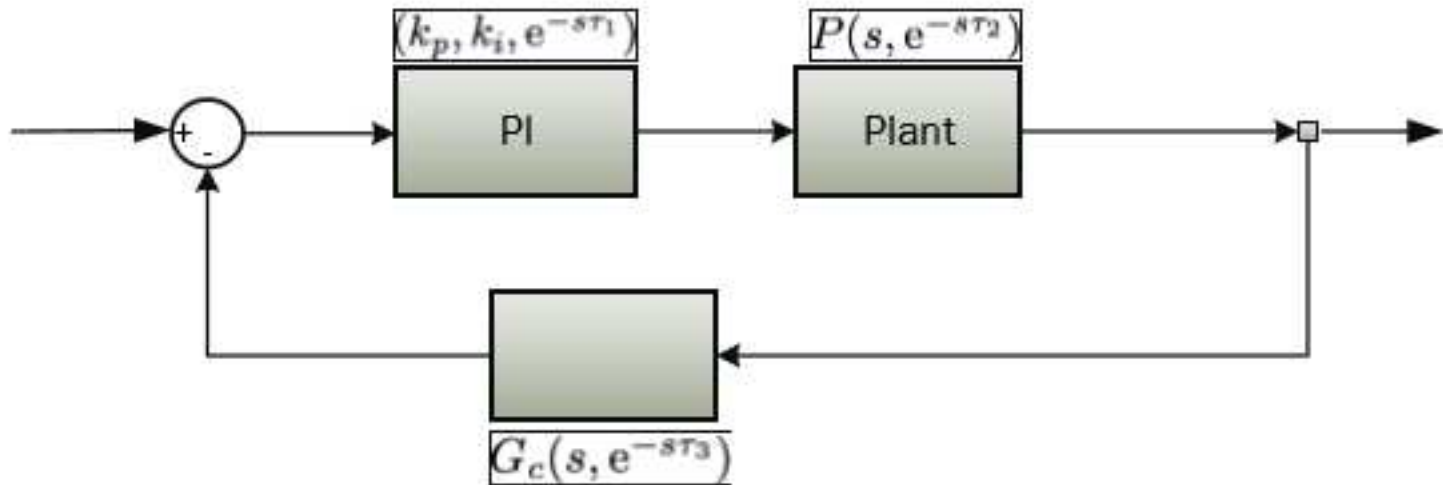
ACKNOWLEDGMENT

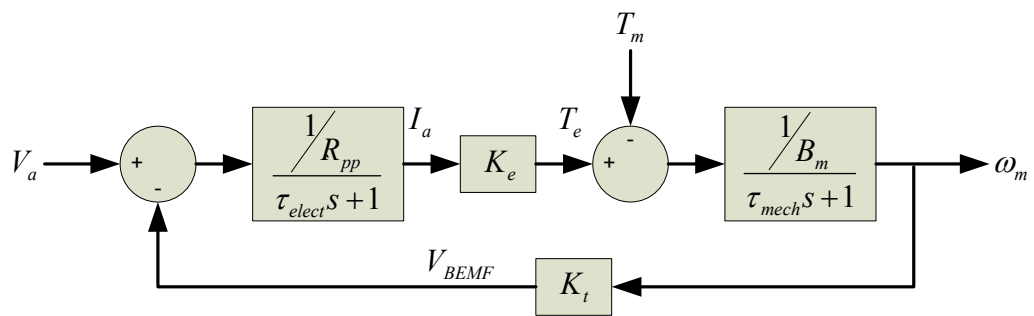
This research work was supported in part by the Natural Sciences and Engineering Research Council of Canada NSERC/Engage Program and the National Research Council Canada NRC/IRAP Program.

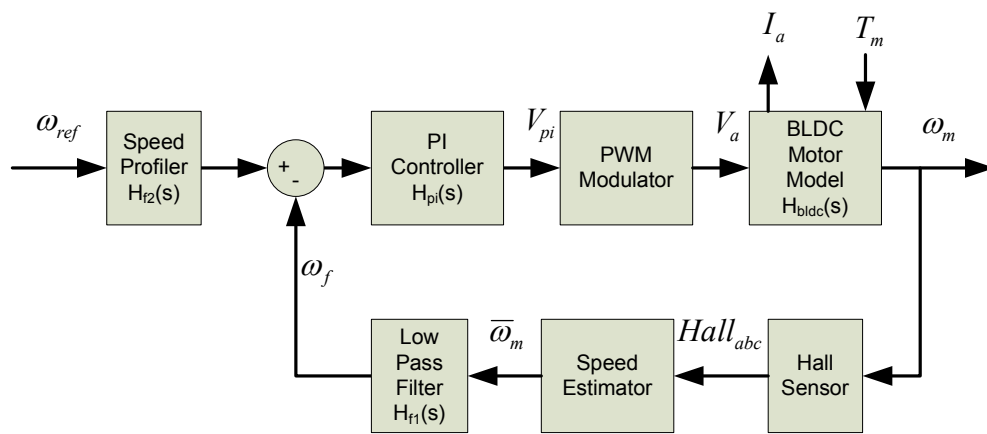
REFERENCES

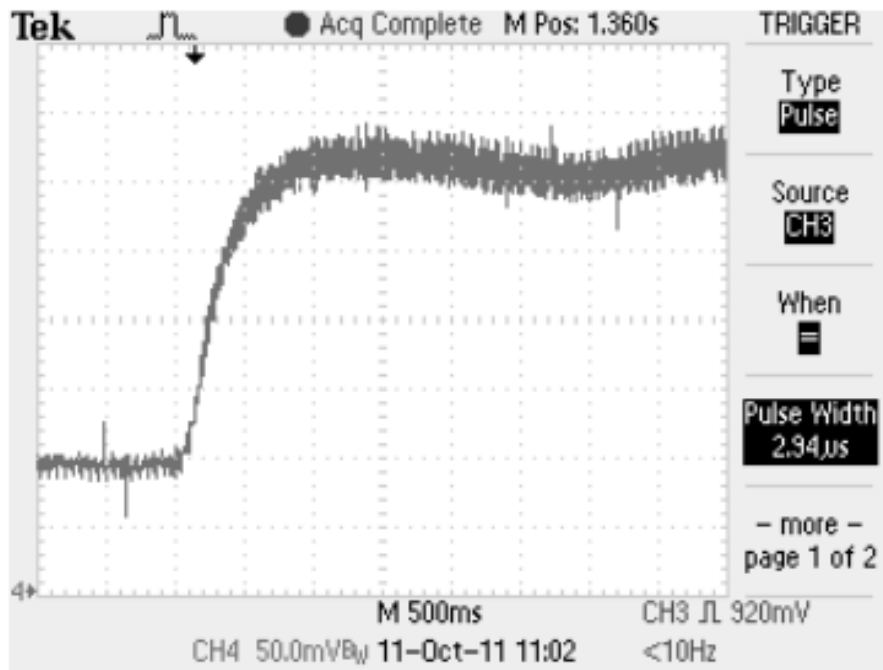
- [1] C.-L. Xia, *Permanent Magnet Brushless DC Motor Drives and Controls*. Beijing, China: Wiley Press, 2012.
- [2] R. Krishnan, *Permanent Magnet Synchronous and Brushless DC Motor Drives*. Florida, USA: CRC Press, 2009.
- [3] T. W. Chun, Q. V. Tran, H. H. Lee, and H. G. Kim, "Sensorless control of bldc motor drive for an automotive fuel pump using a hysteresis comparator," *IEEE Trans. on Power Electronics*, vol. 29, no. 3, pp. 1382–1391, March 2014.

- [4] D. Collins, P. Anderson, S. Beyer, and D. Moreno, "Brushless motors for in-tank fuel pumps," in *Proceedings of the SAE 2012 World Congress & Exhibition*. PA, USA: SAE International, Apr. 2012, pp. 2012–01–0426.
- [5] M. Gougani, M. Chapariha, J. Jatskevich, and A. Davoudi, "Hall sensor-based locking electric differential system for bldc motor driven electric vehicles," in *Proceedings of IEEE International Electric Vehicle Conference (IEVC2012)*. NJ, USA: IEEE, March 2012, pp. 1–7.
- [6] A. Vanisri and N. Devarajan, "Torque ripple minimization in indirect position detection of permanent magnet brushless dc motor," *European Journal of Scientific Research*, vol. 65, no. 4, pp. 481–489, Dec. 2011.
- [7] Z. Kolondzovski, A. Arkkio, J. Larjola, and P. Sallinen, "Power limits of highspeed permanent magnet electrical machines for compressor applications," Aalto Univ., School of Sci. and Tech., Tech. Rep., 2010.
- [8] G. F. Franklin, P. J. D., and W. M., *Digital Control of Dynamic Systems*, 3rd ed. Addison-Wesley, 1998.
- [9] K. Ogata, *Discrete-Time Control Systems*, 2nd ed. Prentice-Hall, 1995.
- [10] N. Olgac and R. Sipahi, "An exact method for the stability analysis of time delayed lti systems," *IEEE Transactions on Automatic Control*, vol. 47, no. 5, pp. 793–797, May 2002.
- [11] —, "A practical method for analyzing the stability of neutral type lti-time delayed systems," *Automatica*, vol. 40, no. 5, pp. 847–853, May 2004.
- [12] G. Lu, L. F. Yeung, D. W. C. Ho, and Y. Zhang, "Strict positive realness for linear time-invariant systems with time-delays," in *IEEE Conference on Decision and Control*, vol. 5, 2000, pp. 5004–5009.
- [13] S. Niculescu, *Delay effects on stability: A robust control approach*. Springer-verlag, 2001.
- [14] K. Gu, V. L. Karitonov, and J. Chen, *Stability of Time-Delay Systems*. Boston, USA: Birkhauser, 2003.
- [15] S. I. Niculescu and K. Gu, *Advances in Time-Delay Systems*. Berlin, Germany: Springer Verlag, 2004.
- [16] F. M. Atay, *Complex Time-Delay Systems: Theory and Applications*. Berlin, Germany: Springer-Verlag, 2010.
- [17] I. I. Delice and R. Sipahi, "Delay-independent stability test for systems with multiple time-delays," *IEEE Trans. on Automatic Control*, vol. 57, no. 4, pp. 963–972, April 2012.
- [18] L. El Ghaoui and I. I. Niculescu, *Advances in Linear Matrix Inequality Methods in Control*. Philadelphia, USA: SIAM, 2000.
- [19] R. Sipahi and N. Olgac, "A comparative survey in determining the imaginary characteristic roots of lti time delayed systems," in *Proceedings of the 16th IFAC World Congress, 2005*. Laxenburg, AT: Elsevier IFAC, Jul 2005, pp. 635–635.
- [20] M. Laughton and D. Warne, *Electrical Engineers Reference Book*. Elsevier Science, 2002.
- [21] M. G. Simoes and P. V. Jr., "A high-torque low-speed multiphase brushless machine - a perspective application for electric vehicles," *IEEE Transactions on Industrial Electronics*, vol. 49, no. 5, pp. 1154–1164, Aug 2002.
- [22] T.-Y. Kima, B.-K. Leeb, and C.-Y. Wonb, "Modeling and simulation of multiphase bldc motor drive systems for autonomous underwater vehicles," in *IEEE International Conference on Electrical Machines and Drives - IEMDC*, May 2007, pp. 1366–1371.
- [23] S. Kim, "Modeling and fault analysis of bldc motor based servo actuators for manipulators," in *IEEE International Conference on Robotics and Automation - ICRA*, May 2008, pp. 767–772.
- [24] T. I. Inc., *Stellaris Brushless DC (BLDC) Motor Control Reference Design Kit with Ethernet and CAN - User's Manual, Rev. C*. Texas Instrument Inc., 108 Wild Basin, Suite 350, Austin, TX 78746, Feb. 2010, rDK-BLDC-UM-07.
- [25] D. Xue, Y. Chen, and D. P. Atherton, *Linear Feedback Control: Analysis and Design with MATLAB*. Philadelphia, USA: SIAM, 2007.

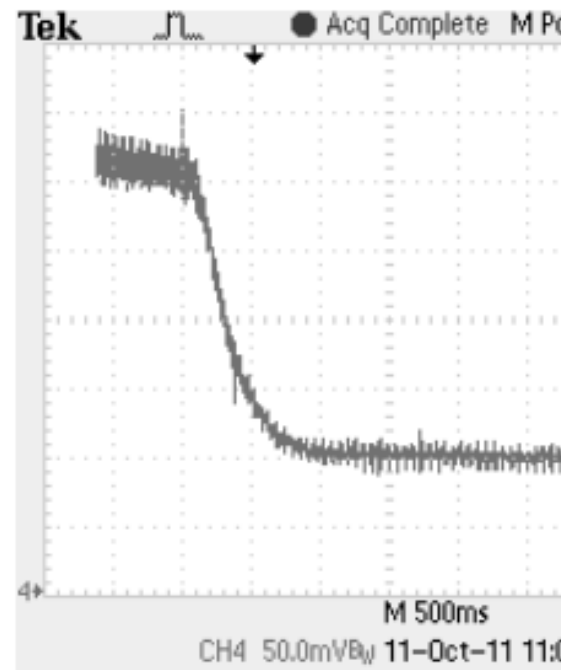




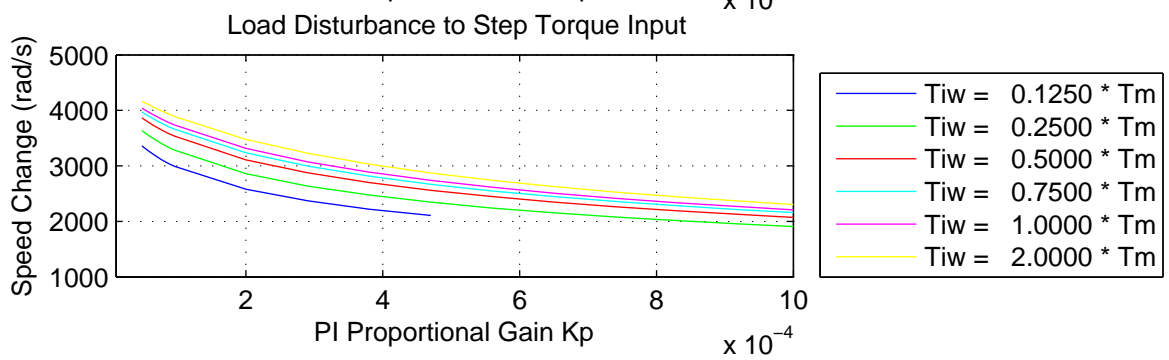
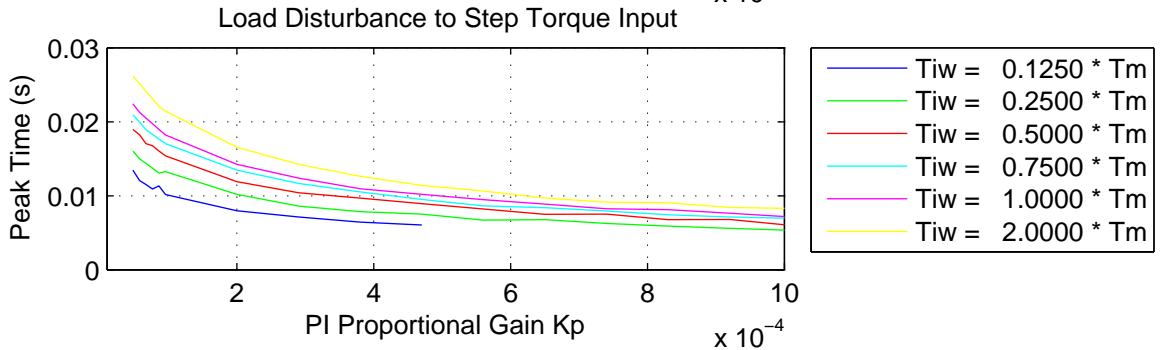
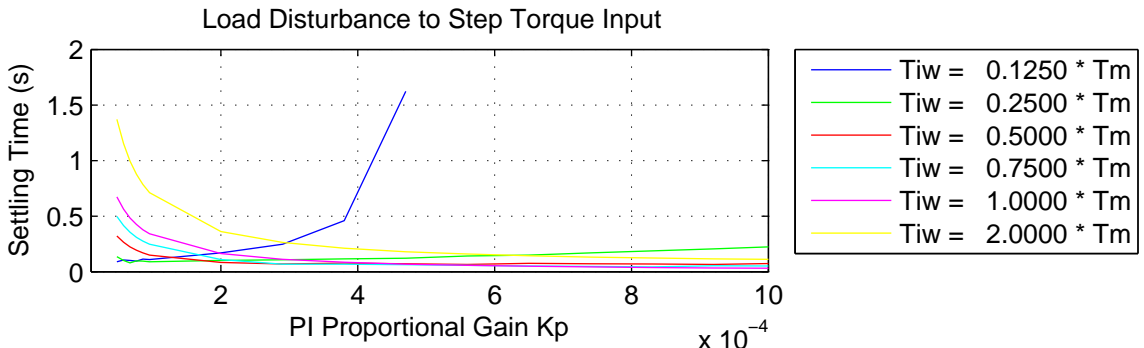


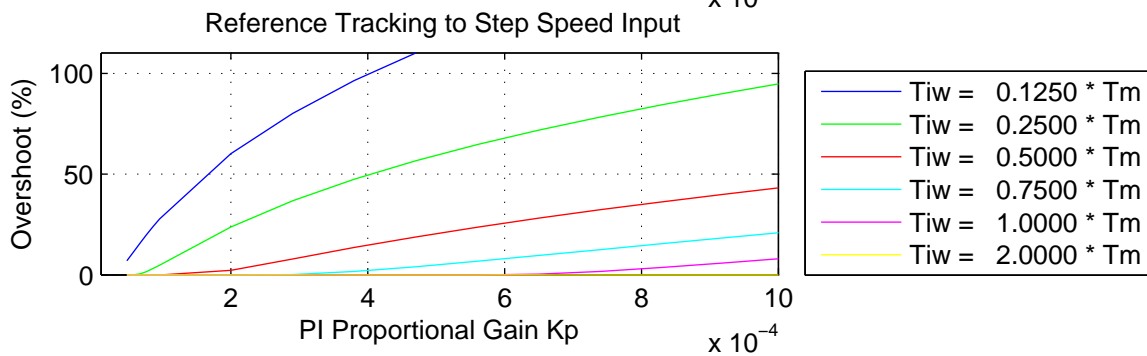
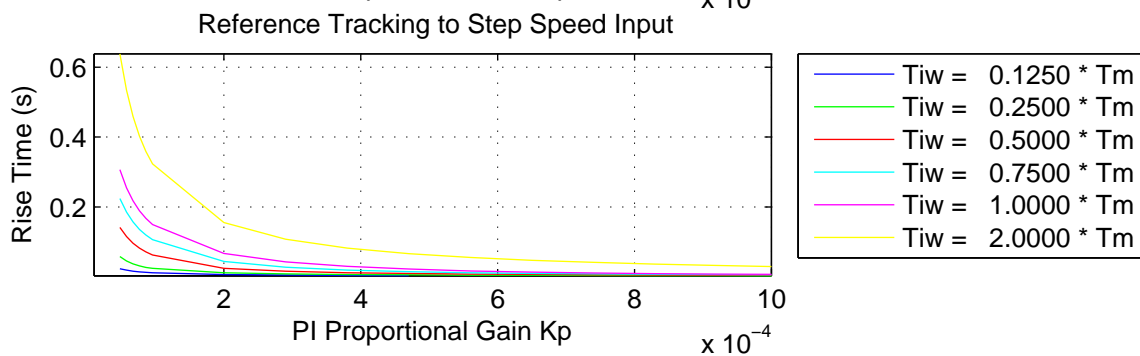
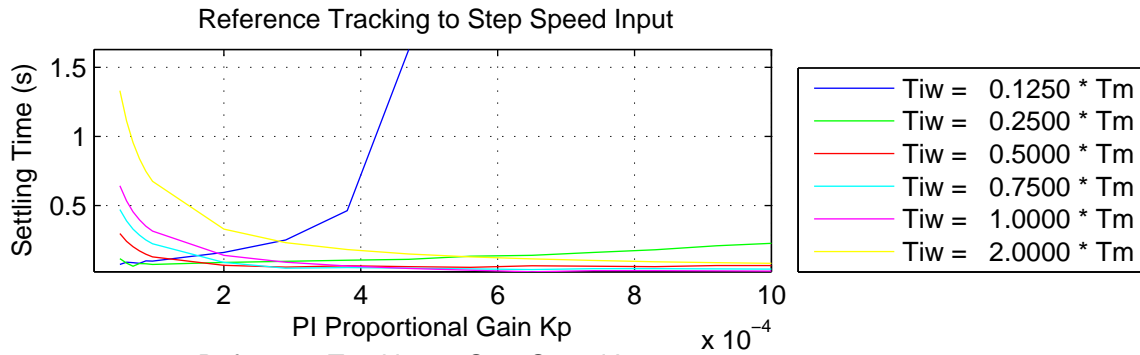


TPS 2024 - 11:11:22 PM 10/10/2011

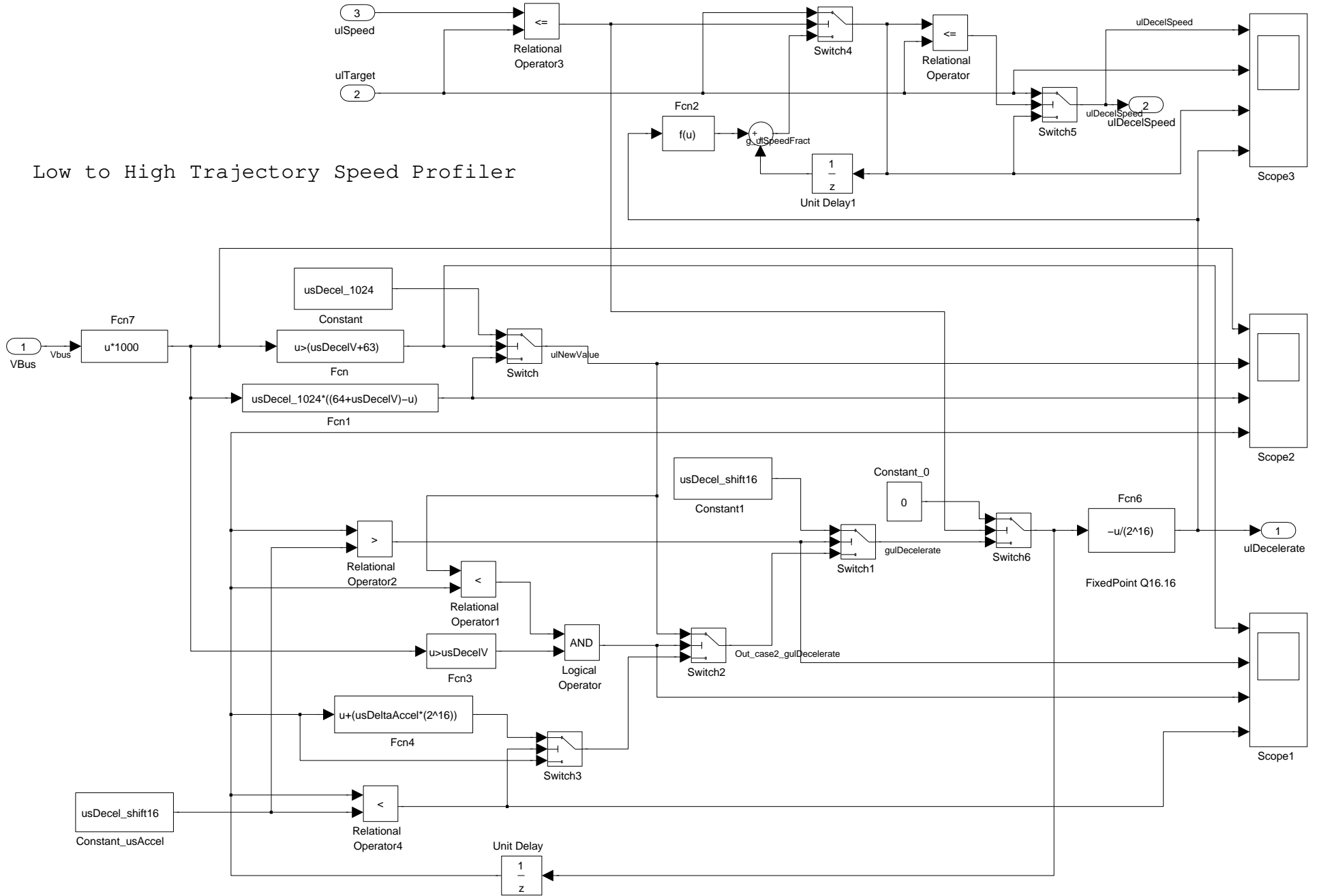


TPS 2024 - 11:15:18 PM 10/10/2011

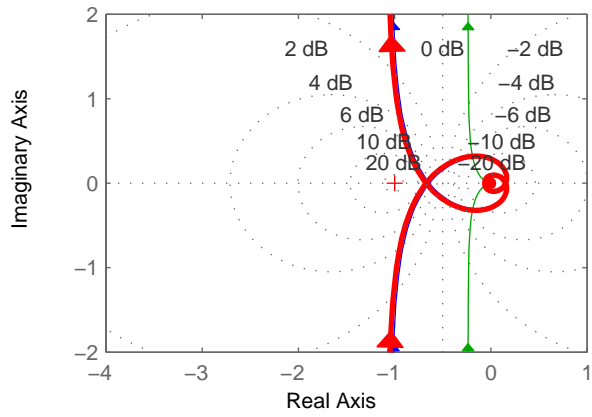




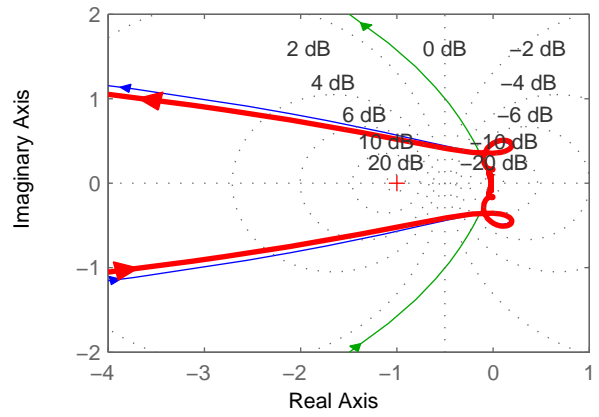
Low to High Trajectory Speed Profiler



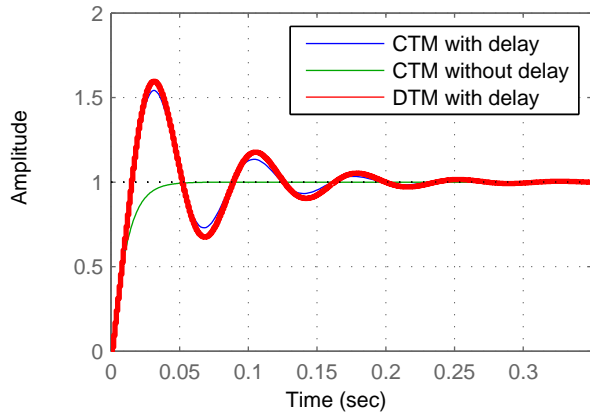
Set-Point Tracking Nyquist Curve



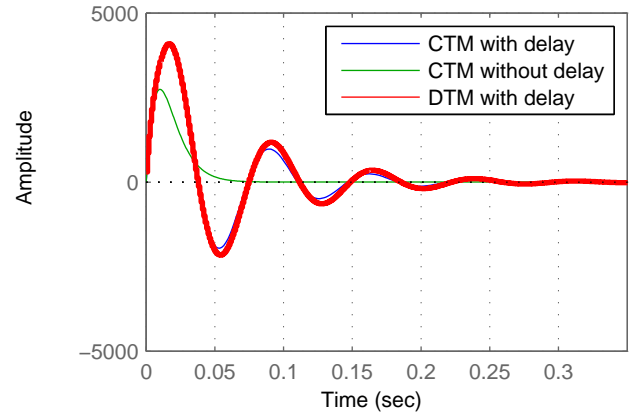
Load Disturbance Nyquist Curve



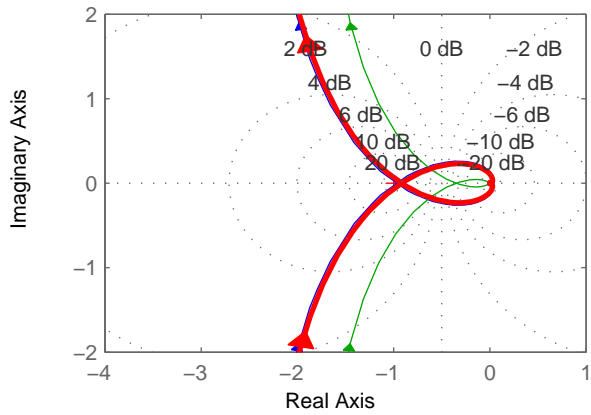
Step Response: ($w=1\text{kRPM}$, $T_s=1\text{ms}$)



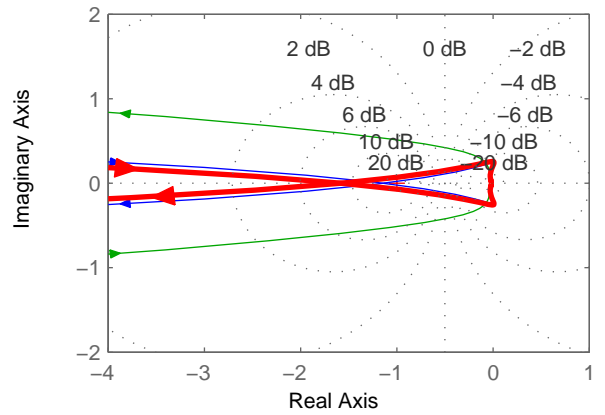
Step Response: ($w=1\text{kRPM}$, $T_s=1\text{ms}$)



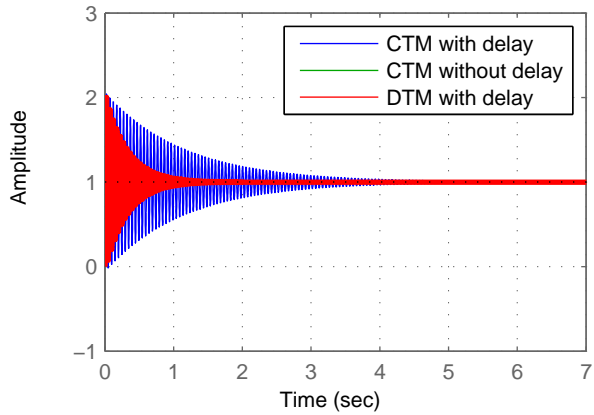
Set-Point Tracking Nyquist Curve



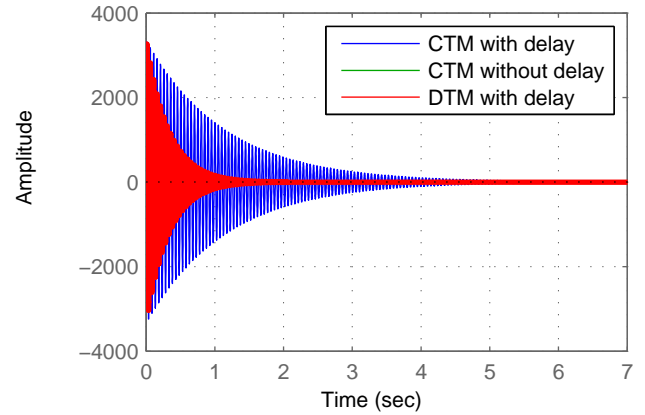
Load Disturbance Nyquist Curve



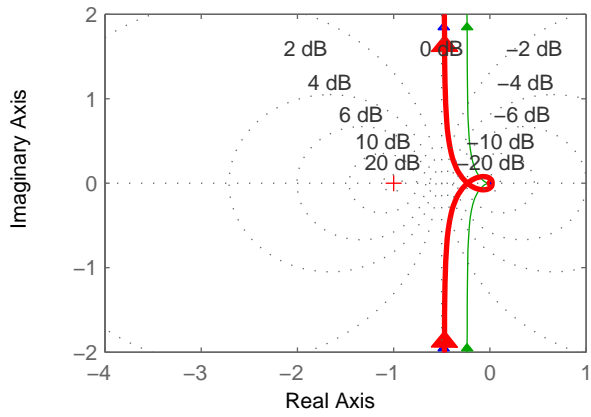
Step Response: ($\omega=6\text{kRPM}$, $T_s=1\text{ms}$)



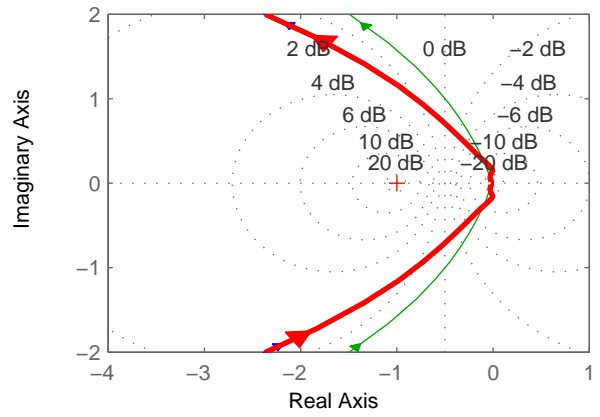
Step Response: ($\omega=6\text{kRPM}$, $T_s=1\text{ms}$)



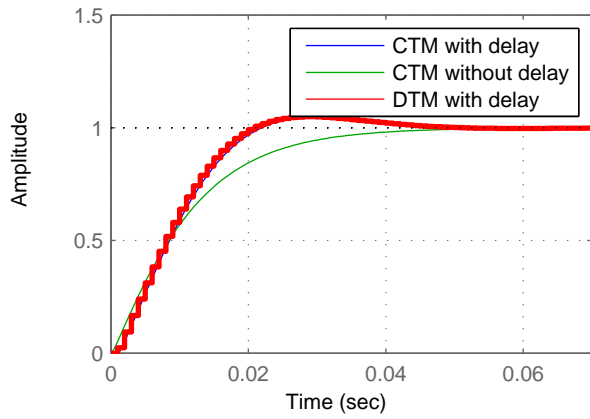
Set-Point Tracking Nyquist Curve



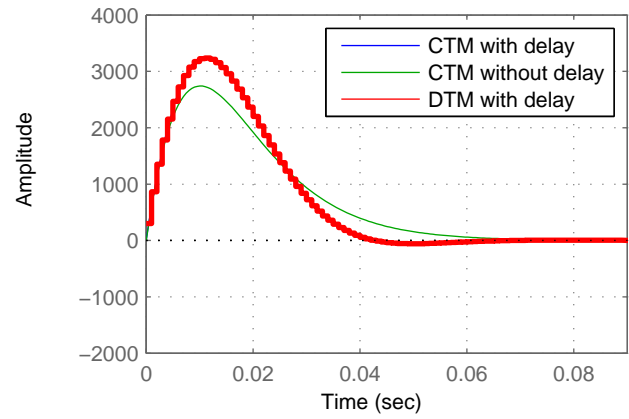
Load Disturbance Nyquist Curve



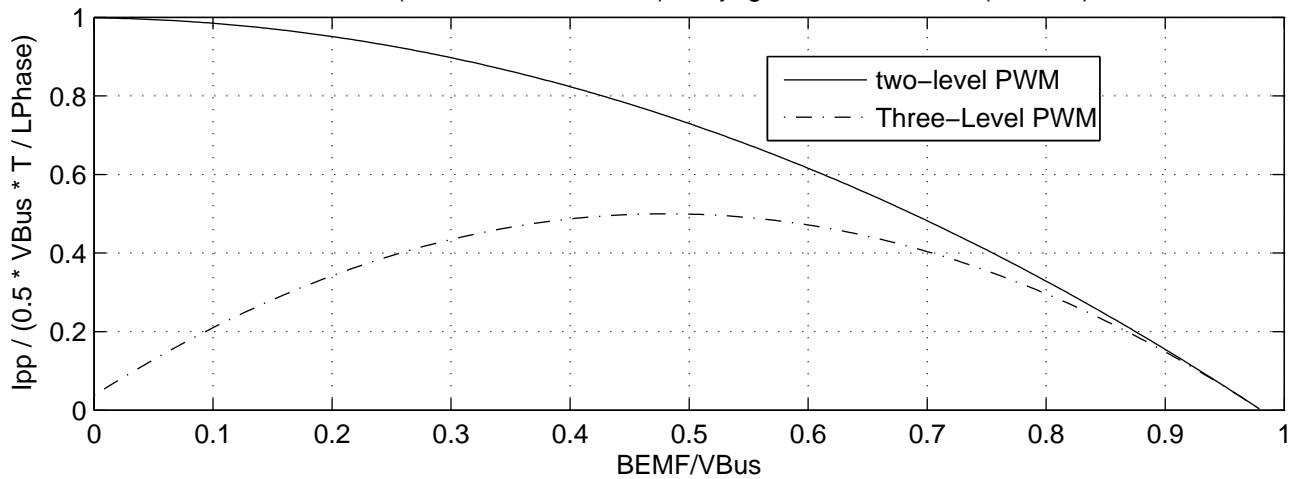
Step Response: ($\omega=6\text{kRPM}$, $T_s=1\text{ms}$)



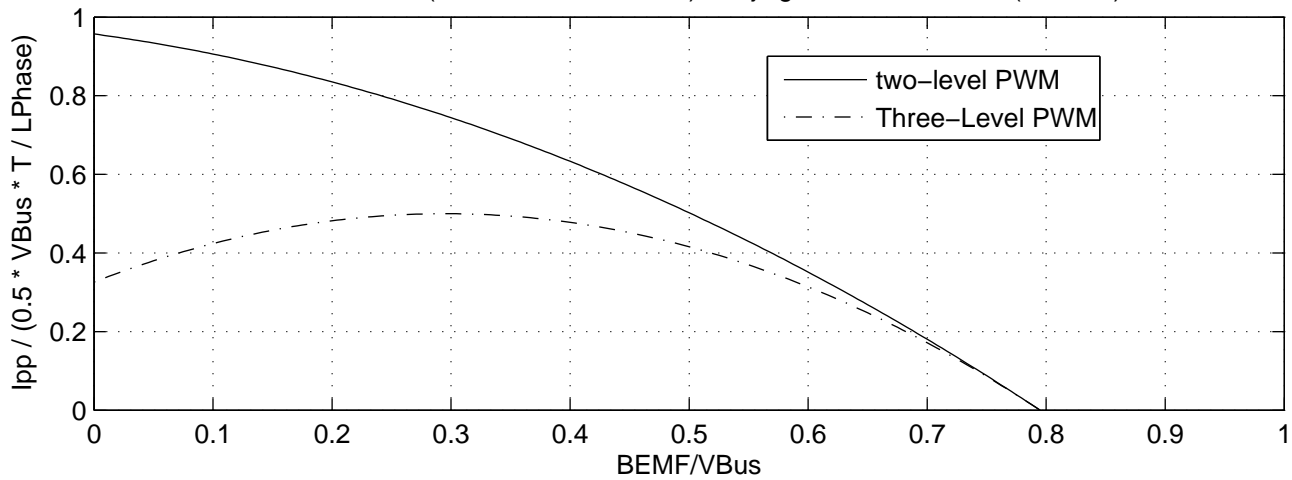
Step Response: ($\omega=6\text{kRPM}$, $T_s=1\text{ms}$)

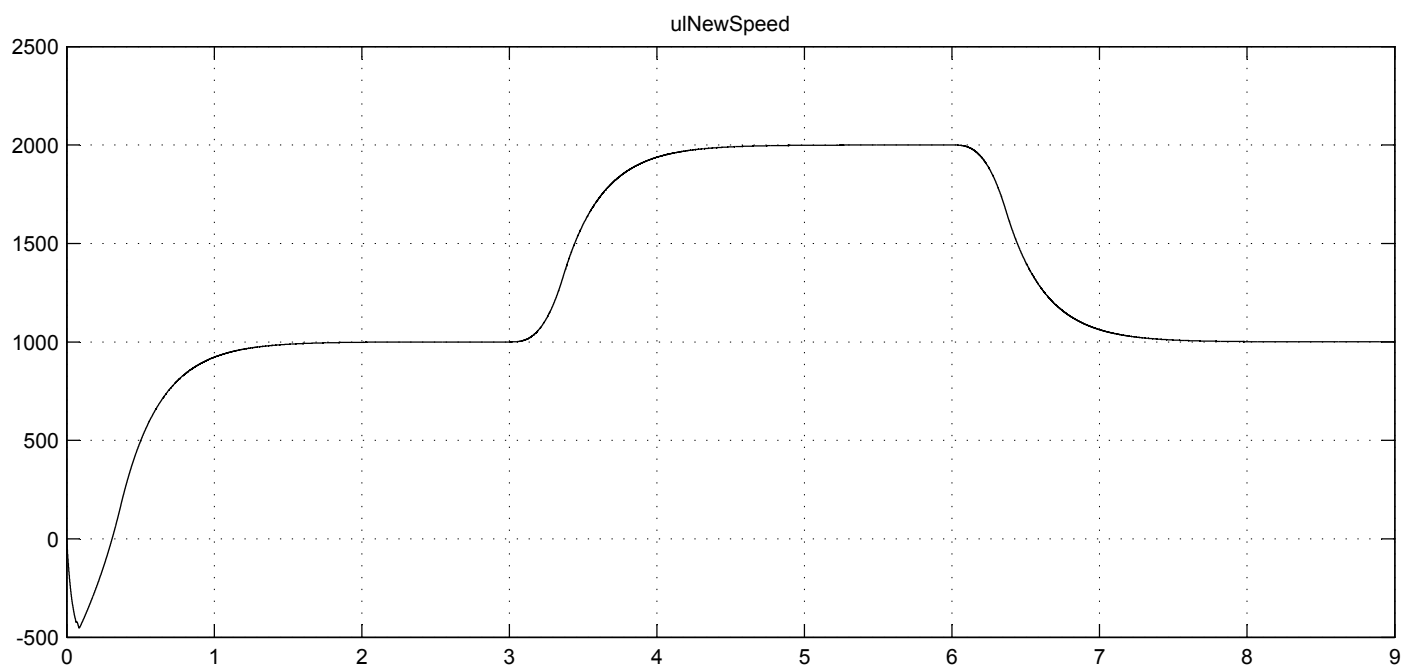
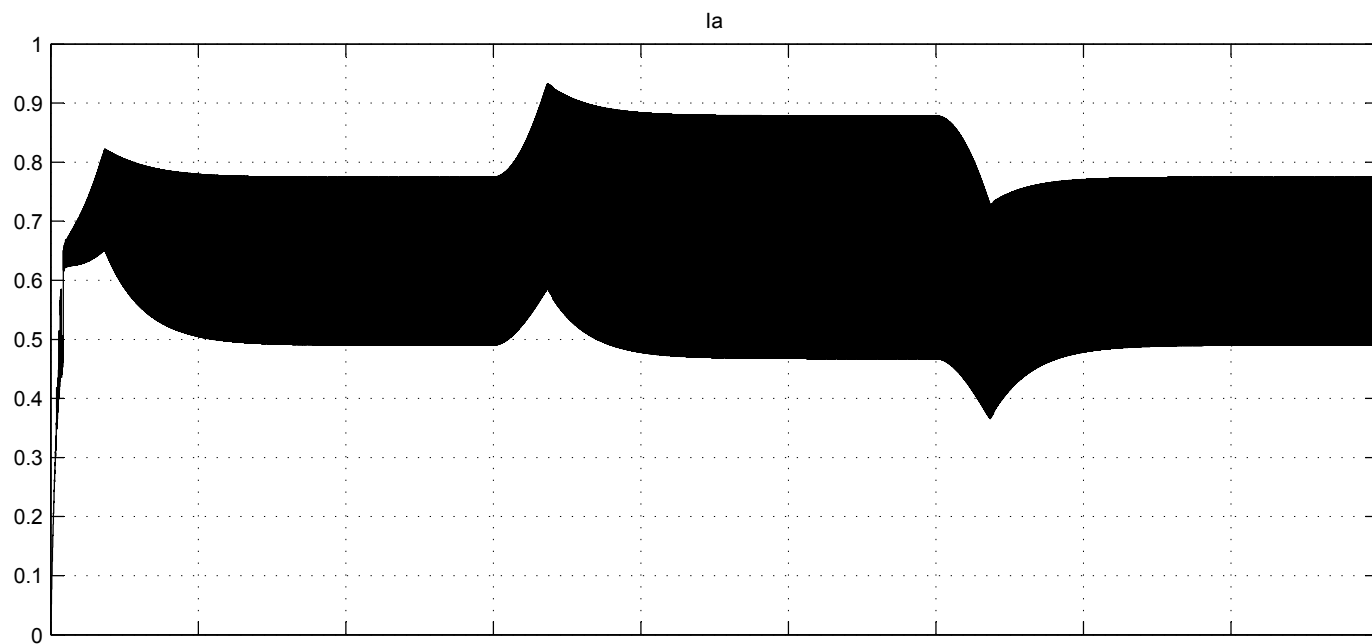


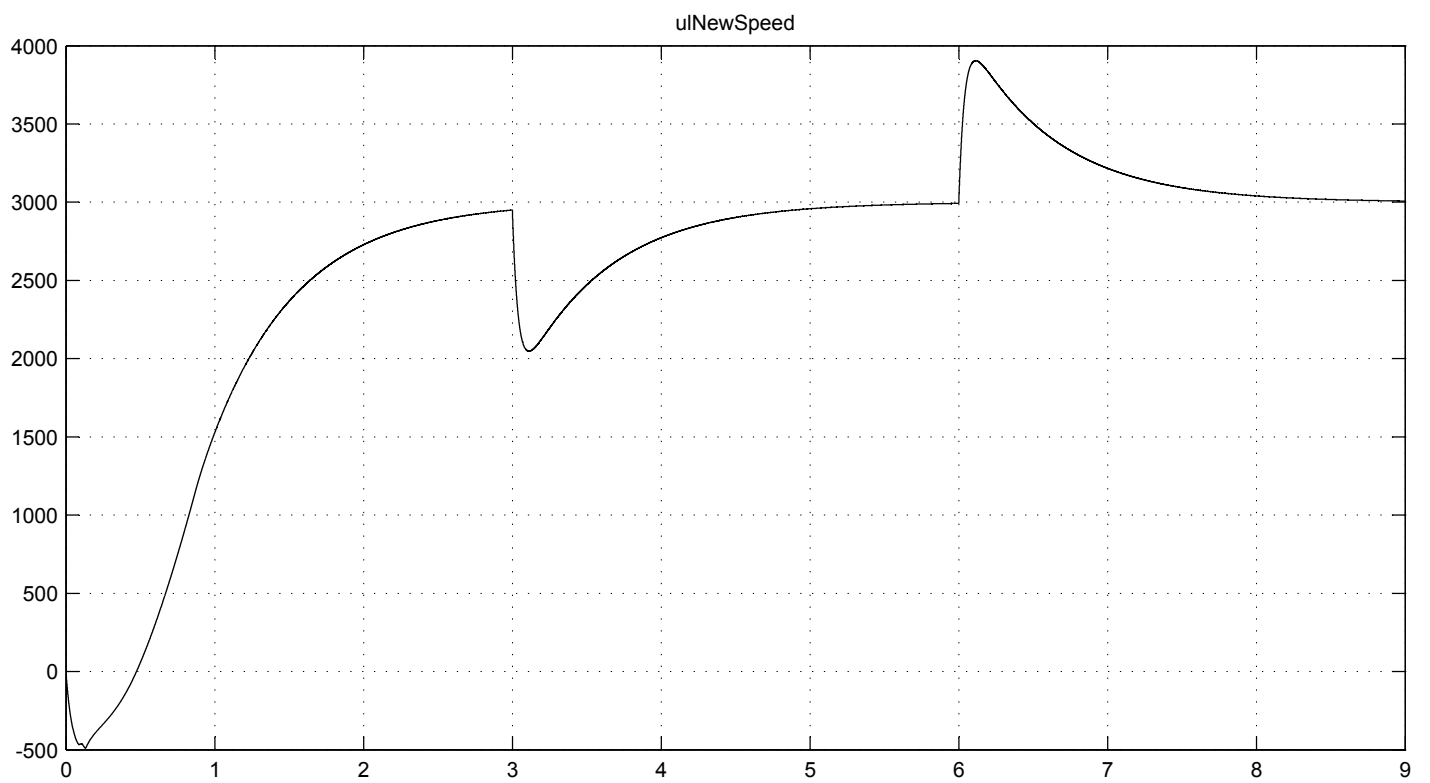
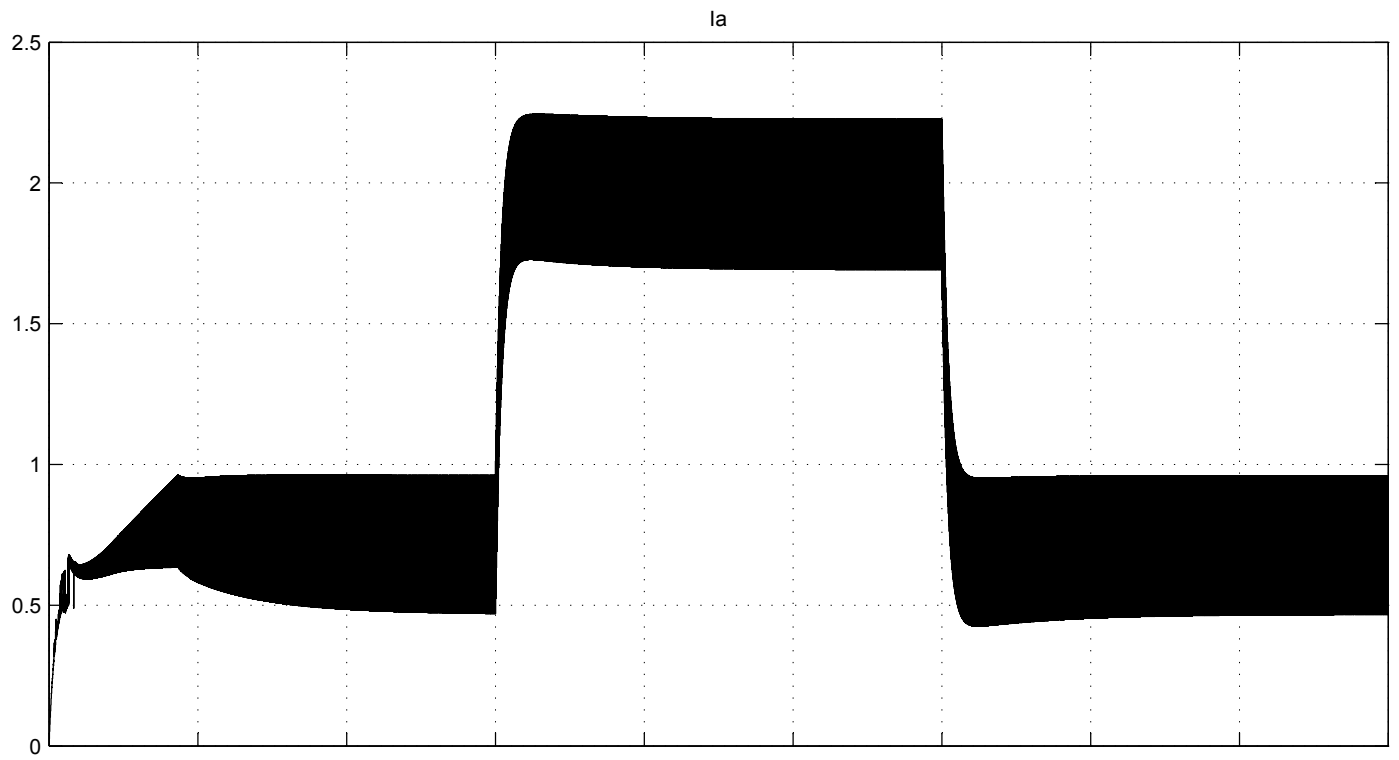
No-load:(I=0.2A N=10080RPM)-Beijing Motors Inc. Model(BL3056)

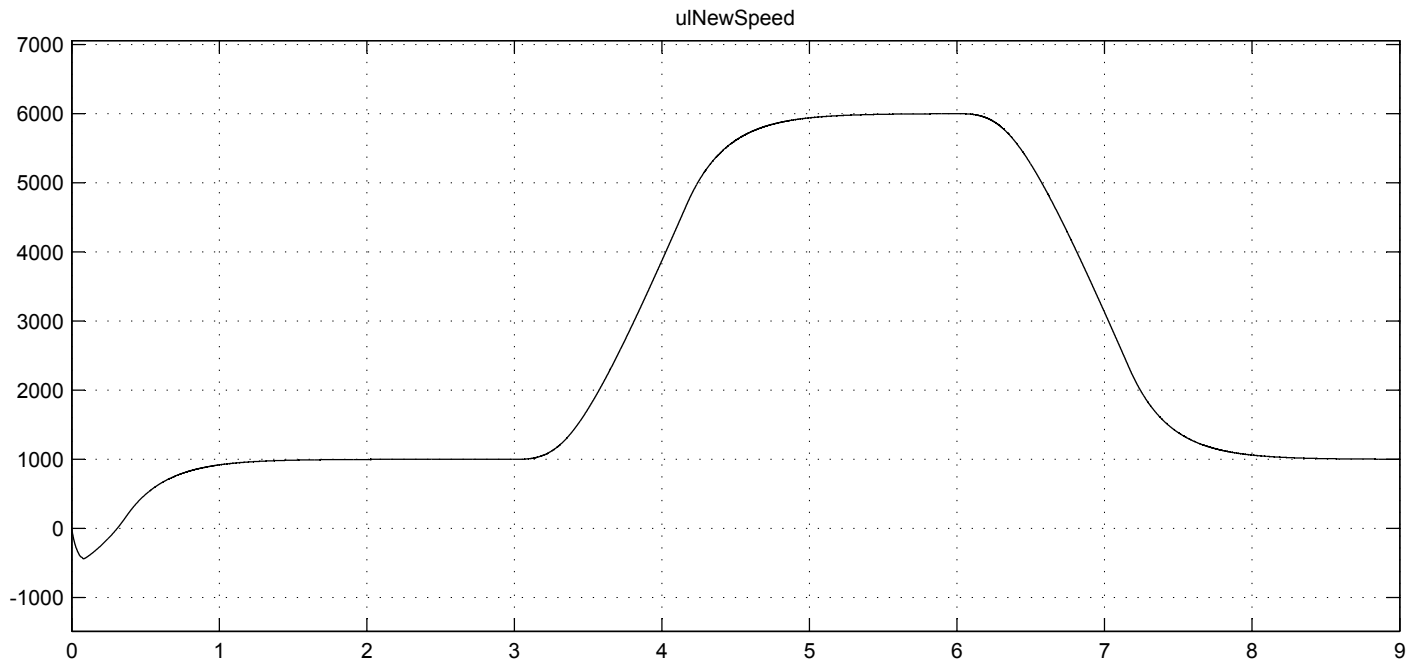
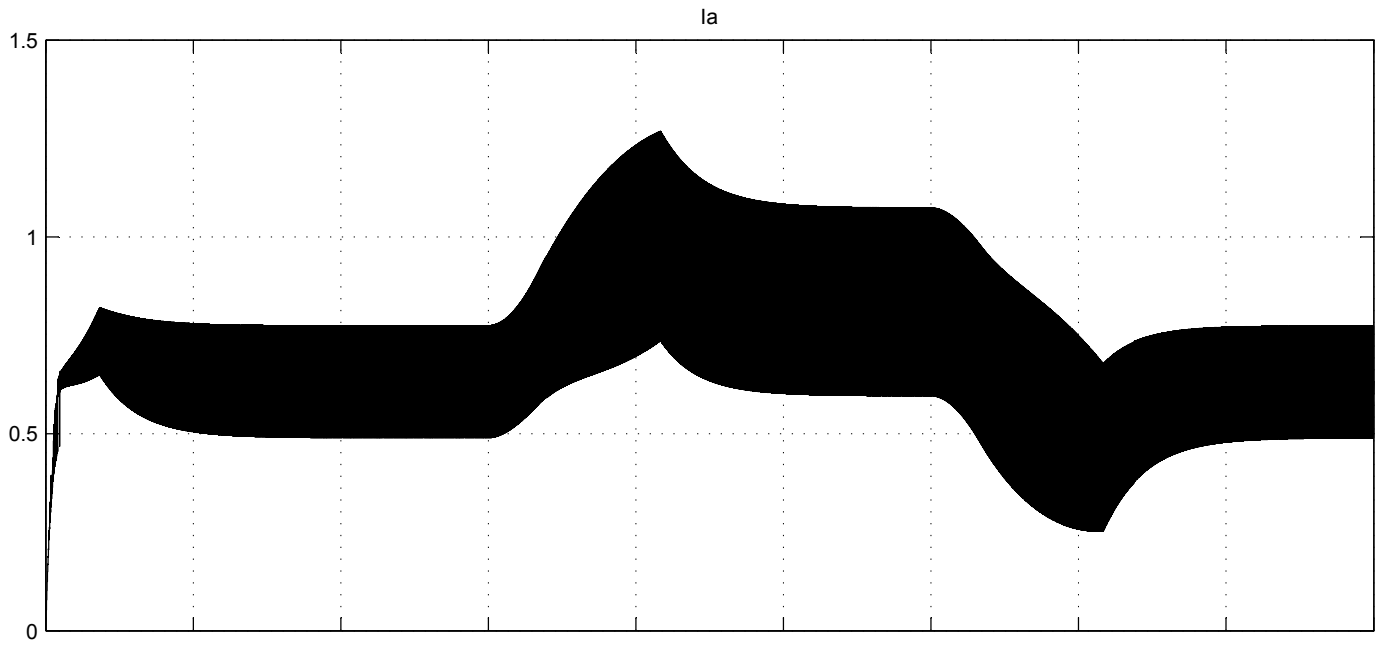


Rated current:(I=2.14A N=8671RPM)-Beijing Motors Inc. Model(BL3056)

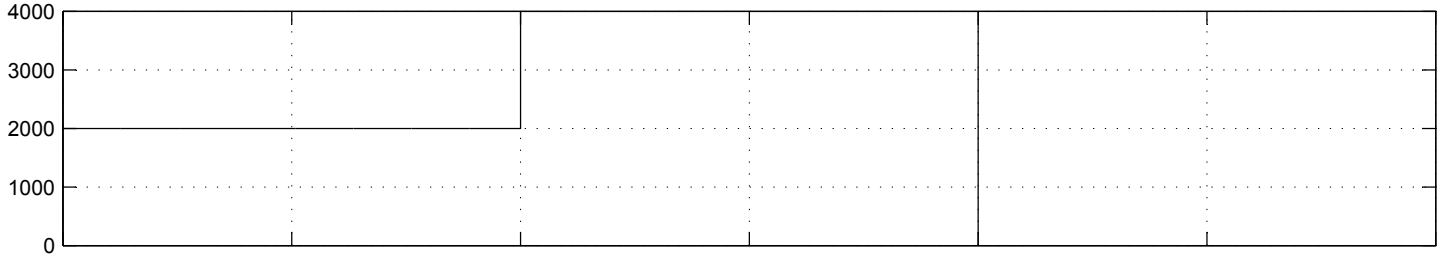




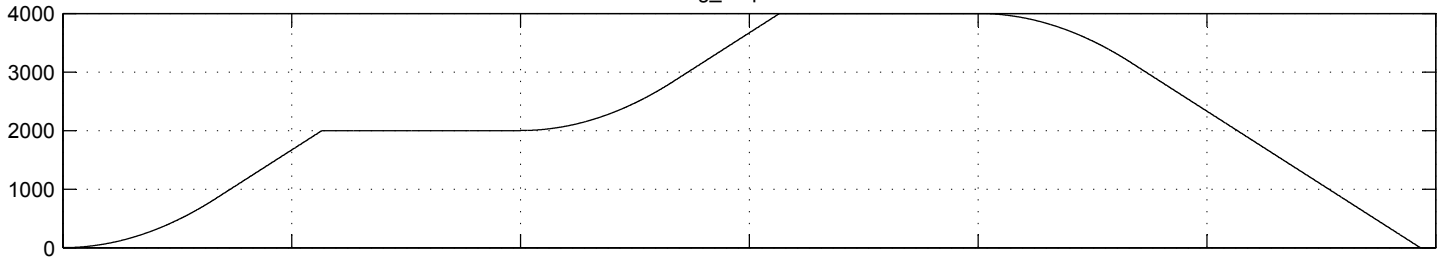




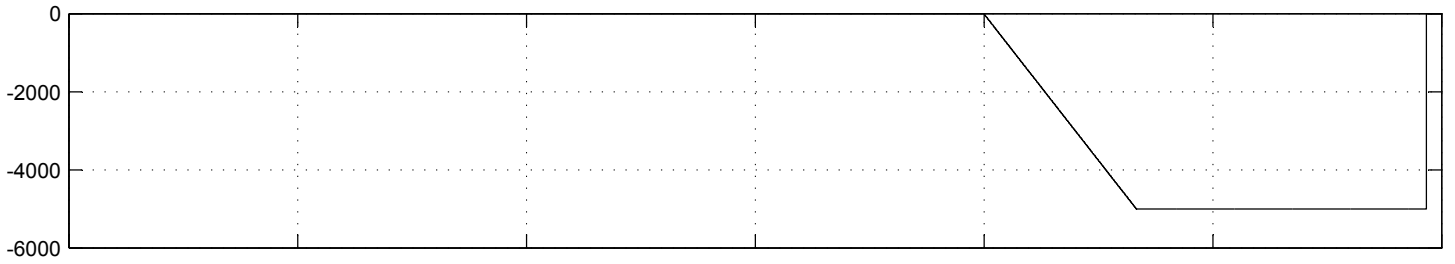
uITarget



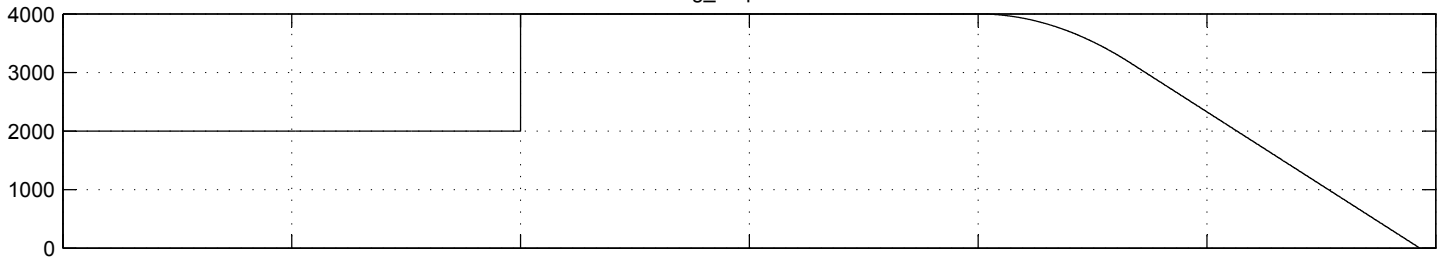
g_ulSpeed



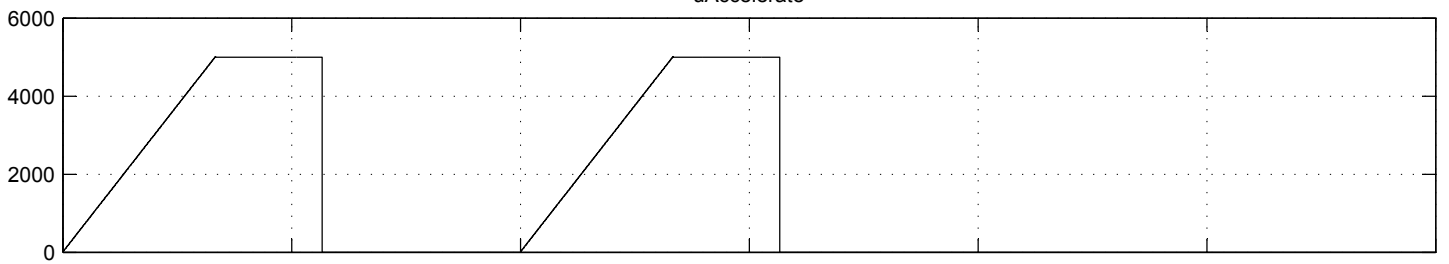
uDecelerate



g_ulSpeed2



uAccelerate



g_ulSpeed1

